Paclitaxel induces immunogenic cell death in ovarian cancer via TLR4/IKK2/SNARE-dependent exocytosis

Tat-San Lau[1], Loucia Kit-Ying Chan[1], Gene Chi-Wan Man[2], Eric Chi-Hang Wong[3], Jacqueline Ho-Sze Lee[1], So-Fan Yim[1], Tak-Hong Cheung[1], Iain McNeish[4], Joseph Kwong[1]

[1]Department of Obstetrics and Gynaecology, Faculty of Medicine, The Chinese University of Hong Kong, Hong Kong, China

[2]Department of Orthopaedics and Traumatology, Faculty of Medicine, The Chinese University of Hong Kong, Hong Kong, China

[3]Department of Clinical Oncology, Faculty of Medicine, The Chinese University of Hong Kong, Hong Kong, China

[4]Department of Surgery & Cancer, Faculty of Medicine, Imperial College London, London, United Kingdom

Running title: Paclitaxel induces immunogenic cell death via TLR4 in cancer cells

Keywords: Paclitaxel, Immunogenic cell death, Ovarian cancer, TLR4 signaling, SNARE-dependent exocytosis

This research was supported by Hong Kong Research Grant Council General Research Fund (467713 and 14109515), and CUHK Research Committee Funding (Direct Grants for Research 4054185, 4054352, and 4054410) to J.K.

Corresponding author: Joseph Kwong
Assistant Professor,
Department of Obstetrics and Gynaecology,
Faculty of Medicine,
The Chinese University of Hong Kong

Mail address: 1/F, Block E, Prince of Wales Hospital,
Shatin, N.T., Hong Kong, China

Phone number: (852) 3505 2801
Fax number: (852) 2636 0008
Email address: josephkwong@cuhk.edu.hk

The authors declare no potential conflicts of interest.

Abstract

Emerging evidence shows that the efficacy of chemotherapeutic drugs is reliant substantially on their capability of inducing immunogenic cell death (ICD) that transforms dying tumor cells into antitumor vaccines, yet the underlying molecular mechanism remains largely unknown. Our long-term goal is aimed at uncovering potential therapeutic strategies to target ovarian cancer through better understanding of the standard-of-care chemotherapy treatment. Here we showed in ovarian cancer that paclitaxel induces ICD-associated DAMPs (i.e. damage-associated molecular patterns, such as CALR exposure, ATP secretion and HMGB1 release) *in vitro* and elicits significant antitumor responses in tumor vaccination assays *in vivo*. We also reported that paclitaxel-induced TLR4 signaling is essential to the release of DAMPs, which activates NF-κB-mediated CCL2 transcription and IKK2-mediated SNARE-dependent vesicle exocytosis that exposes CALR to cell surface. On the other hand, paclitaxel induces ER stress that triggers PERK activation and eIF2α phosphorylation independent of TLR4. Further studies showed that the presence of cytotoxic T lymphocytes is associated with tumor samples from ovarian cancer patients with neoadjuvant chemotherapy; CALR expressions in primary ovarian tumors are also correlated with patients' survival and chemotherapy responses. These findings thus uncover the effectiveness of paclitaxel relies upon the activation of antitumor immunity by inducing ICD via TLR4 and highlight the importance of CALR expressions in cancer cells as the indicators of response to paclitaxel chemotherapy in ovarian cancer.

Introduction

New insights into ovarian cancer treatment is indispensable as the survival of patients presenting with advanced disease has changed little in the past 30 years (1). A combination of tumor debulking surgery and chemotherapy has remained as the standard-of-care treatments (2), whilst chemotherapy management has evolved from a single agent to combination regimen over the last 50 years. Cisplatin was the primary chemotherapeutic agent in the late 1970s, while carboplatin was introduced in the 1990s as an analog of cisplatin with similar effectiveness but considerably less toxicity. Nevertheless, paclitaxel introduced in the late 1990s has changed the standard treatment for ovarian cancer. Randomized clinical trials in advanced disease patients showed better efficacy and tolerability with the combination of carboplatin and paclitaxel, supporting such combinatorial regimen as the standard for treating advanced ovarian cancer nowadays (3).

The efficacy of most widely used chemotherapeutic agents relies on targeting, i.e. inducing apoptosis, of all tumor cells, but with side effects of exerting immunosuppressive response after initial treatment that renders the tumor cell variants escaping from chemotherapy. In contrast, increasing evidence has been indicating the induction of innate and adaptive antitumor immune responses is decisive in determining the success of chemotherapy. In 2005, Kroemer and colleagues discovered that the apoptosis triggered by certain types of chemotherapeutics agents could convert the dying tumor cells to elicit immune responses, a phenomenon referred to as “immunogenic cell death” (ICD) which contributes to the elimination of residual tumor cells (4, 5). Their vaccination experiments in mice showed a limited number of cytotoxic agents that are currently used in the clinic (including doxorubicin, mitoxantrone, oxaliplatin and bortezomib) induced mouse tumor cells to undergo *bona fide* ICD (6). Studies have also shown the chemotherapy-driven ICD

relies on the release or exposure of potential immunogenic signals known as “damage-associated molecular patterns” (DAMPs) from dying cells to induce immune responses. To-date, ICD is characterized by multiple key DAMPs, including exposure of endoplasmic reticulum (ER) chaperones, such as calreticulin (CALR) (7), ERp57 (protein disulfide isomerase family A member 3; also known as PD1A3) (8), heat shock protein 70kDa (HSP70) and heat shock protein 90kDa (HSP90) (9) on the plasma membrane of dying tumor cells; secretion of adenosine triphosphate (ATP) (10), high-mobility group box 1 (HMGB1) (11) and annexin A1 (ANXA1) (12); and activation of the cancer cell-intrinsic type I interferon (IFN) response and consequent secretion of the chemokine (C-X-C motif) ligand 10 (CXCL10) (13). These DAMPs, upon binding to their own receptors on the surface of myeloid and lymphocytes cells, favor the recruitment, activation, homing, antigen uptake and maturation of antigen presenting cells, i.e. dendritic cells. These processes could eventually prime the activation of an adaptive immune response involving T cells, which may eliminate tumor cells that survive chemotherapy via IFN-γ-dependent manner (6).

Calreticulin (CALR) is the first key player identified in inducing ICD in cancer. With anthracycline treatment, CALR is translocated rapidly from ER to the cell surface of pre-apoptotic tumor cells. Exposure of CALR renders the anthracycline-treated tumor cells being recognized and phagocytosed by dendritic cells and enhances their immunogenicity in mice (7). Thus, the cell surface exposure of CALR in ICD serves not only as an important “eat me” signal for dendritic cells, but also a crucial inducer of antitumor immune response (14, 15). Additionally, ERp57 is an ER-sessile protein that co-translocates with CALR to the cell surface of anthracycline-treated tumor cells (8).

The release of ATP, HMGB1 and ANXA1 by dying tumor cells is also associated with chemotherapy-induced ICD that elicits antitumor immunity driven by intratumoral dendritic cells. ATP secretion was found to attract and bind to P2X7 purinergic receptors on dendritic cells and activates the NLR family, pyrin domain containing 3 (NLRP3) inflammasome, allowing interleukin-1β (IL-1β) secretion by dendritic cells that primes the IFN-γ-producing CD8+ T cells (10). Another study reported that anthracyclines induce tumor infiltration via ATP release, which recruits myeloid cells into tumors and stimulates the local differentiation of inflammatory dendritic cells with a $CD11c^{+}CD11b^{+}Ly6c^{hi}$ phenotype. These dendritic-like cells can present tumor antigens to T cells and induce antitumor immune responses (16). Besides, studies in mice and human revealed that the immunogenicity of dying tumor cells after chemotherapy or radiotherapy depends on their release of the alarmin protein HMGB1, which activates tumor antigen-specific T cell immunity via the innate receptor Toll-like receptor 4 (TLR4) along with adaptor myeloid differentiation primary response protein-88 (MyD88) expressed by the dendritic cells (11). Additionally, ANXA1 released by dying tumor cells with anthracycline treatment requires interaction with the formyl peptide receptor 1 (FPR1) on dendritic cells to elicit T-cell mediated antitumor immunity (12).

Furthermore, studies showed that anthracyclines activate the endosomal pattern recognition receptor TLR3, which in turn stimulates the rapid production of IFNs by tumor cells. By binding to IFN-α and IFN-β receptors (IFNARs) on tumor cells, type I IFNs trigger autocrine and paracrine circuits that result in the release of CXCL10 (13). CXCL10 was thus considered as an essential chemotactic factor for the recruitment of immune effectors that selectively attack the tumor (17).

In this study, we investigated if the standard-of-care chemotherapy (carboplatin and paclitaxel) induces ICD in ovarian cancer. We found that paclitaxel, but not carboplatin, induces ICD in syngeneic murine models of ovarian cancer via TLR4-independent and -dependent pathways.

Materials and Methods

Patients and Specimens. One hundred and twenty four patients with epithelial ovarian cancer (EOC) after primary debulking surgery and 9 patients with advanced ovarian cancer after neoadjuvant chemotherapy (NACT) followed by interval debulking surgery (1 received carboplatin monotherapy and 8 received paclitaxel-carboplatin regimen) were recruited at the Department of Obstetrics and Gynaecology, The Chinese University of Hong Kong, Prince of Wales Hospital, Hong Kong. Informed written consent was obtained from each patient prior surgery. Clinical parameters of the 124 ovarian cancer patients with primary debulking surgery were summarized in Supplementary Table S1. Ovarian tumor tissues were obtained during surgery and processed further for paraffin-embedded formalin-fixed and OCT-embedded frozen tissues. Histological typing of the ovarian tumors was classified by pathologists according to the World Health Organization criteria, whereas clinical staging was given by gynecologic oncologists following the International Federation of Gynecology and Obstetrics (FIGO) staging system. The research protocol was approved by the institution's Clinical Research Ethics Committee.

Cell lines and cell culture conditions. ID8 cells, ID8F3 cells (a murine model of HGSOC by generating novel ID8 derivatives that harbor Trp53-/- suppressor gene deletion (18)) were cultured in Dulbecco's modified eagle medium (DMEM) supplemented with 4% fetal bovine serum (FBS), 5 ng/mL insulin transferrin sodium selenite and 100 U/ml penicillin and streptomycin. TKO cells (generated from triple-mutant mice that have developed metastatic HGSOC originating from fallopian tube (19)) were cultured in RPMI (Rosewell Park Memorial Institute) medium supplemented with 10% fetal FBS and 100 U/ml penicillin and streptomycin. Unless otherwise specified, all cancer cell lines were maintained at 37 °C under 5% CO_2.

Treatment with chemotherapeutic drugs and inhibitors. Chemotherapeutic drugs including paclitaxel, cisplatin, carboplatin (all from Greiner Bio-One, Frickenhausen, Germany) and mitoxantrone dihydrochloride (Sigma-Aldrich, St. Louis, MO) were used. In functional blockade assays, cells were pre-treated with TAK-242 (100 nM; MedChem Express, Monmouth Junction, NJ), BAY 11-7082 (1 nM), TPCA-1 (100 nM) or IKK2 inhibitor IV (100 nM) (all from Cayman Chemical, Ann Arnor, Michigan) for 2 hours prior to paclitaxel treatment. Cell viability and apoptosis assays were carried out to confirm that there was no alteration of cell growth nor induction of cell death in cell lines under inhibitor treatment.

Generation of Tlr4 knockout cell line by CRISPR/Cas9. To generate Tlr4 KO with ID8 and ID8F3 cells, murine Tlr4 CRISPR/Cas9 KO plasmid with a Tlr4 HDR plasmid (Santa Cruz Biotechnology, Dallas, Texas) was applied. Briefly, ID8 or ID8F3 cells (1.5×10^5 per transfection) were cultured in 6-well plates for 24 hours. The cells were then co-transfected with CRISPR/Cas9 KO plasmid (1 μg) and HDR plasmid (1 μg) by lipofectamine 2000 (Invitrogen, Carlsbad, CA, USA) for 24 hours. Culture media were replaced with complete medium with puromycin (2 μg/ml) at post-transfection for selecting positive transfectants. Monoclonal cell populations of the transfectants were isolated by limiting dilution and expanded under puromycin treatment. The monoclonal cell population with Tlr4 knockout were then verified by RT-PCR and Western blot analysis.

Cell viability assay. Cell viability was measured by CellTiter-Blue® Cell Viability Assay (Promega, Madison, WI, USA) according to the manufacturer's instruction. Briefly, 1×10^4 of cells per well were seeded in 96-well plates for 24 hours. The cells were then treated with

chemotherapeutic drugs in a dose-dependent manner (0.1 μM to 1000 μM) for 48 hr. After the indicated treatment, the cells were incubated in culture medium containing CellTiter-Blue® Reagent (1:5) at 37°C for 4 hr. Cell viability was determined by recording the absorbance at 595 nm. Percentage of growth inhibition was determined by comparing the difference between percentage of viable cells with and without treatment. Growth inhibition (%) and concentration (μM in log) were arranged on vertical axis and horizontal axis, respectively. The half maximal inhibitory concentration (IC50) is the concentration at which the curve passes through the 50% inhibition level.

Cell apoptosis by flow cytometry. Cell apoptosis was determined using a Dead Cell Apoptosis Kit with Annexin V (AnnV) Alexa Fluor™ 488 & Propidum Iodide (PI) (Invitrogen) by flow cytometry according to the manufacturer's instruction. Briefly, after the indicated treatment, cells were resuspended in 100 μl of annexin-binding buffer containing Annexin V FITC and propidium iodide (PI) (1 x 10^6 cell/ml) and incubated at room temperature for 15 min in dark, followed by adding 400 μl of annexin-binding buffer. Cell staining of Annexin V and PI was detected by a flow cytometer FC500 (Beckman Coulter, Indianapolis, IN, USA) and data was analyzed by a software FlowJo Ver.10 (Tree Star, Inc., Ashland, OR, USA). Annexin V (AnnV) binds to phosphatidylserine (PS), therefore the fluorescently labelled annexin V can be used to detect PS that is exposed on the outside of apoptotic cells. However, Annexin V also stains necrotic cells because these cells have ruptured membranes that allow Annexin V to access through the plasma membrane into the cells. To distinguish between apoptotic cells from necrotic cells, we co-stained the cells with propidium iodide (PI) since PI enters necrotic but not apoptotic cells (20). Therefore, AnnV+PI- represents apoptotic cell death; AnnV-PI+ represents non-apoptotic (mitotic) cell death; and AnnV+PI+ represents necrotic cell death.

Cell cycle analysis by flow cytometry. After the indicated treatment, cells were harvested by trypsinization and washed in PBS. The cells were then fixed in cold 70% ethanol for 30 min at 4 °C. Cell cycle analysis was done by the quantitation of DNA content. The fixed cells were further treated with RNase (5 μg per sample) and DNA in the cells was stained with PI which signal was detected by the flow cytometer FC500.

Detection of cell surface protein by flow cytometry and immunostaining. Cells were first resuspended in complete medium after the indicated treatment and washed with FACS buffer (DMEM with 2% FBS). The cells were incubated in FACS buffer with a specific primary antibody: anti-CALR (1:200; Abcam, Cambridge, UK), anti-ERp57 (1:200; Abcam), anti-ANXA1 (1:200; Abcam), anti-HSP70 (1:200; Cell Signaling Technology, Danvers, MA), anti-HSP90 (1:200; Cell Signaling Technology) or anti-F-actin (1:200; Abcam) on ice for 1 hour. After washing, the cells were incubated with Alexa Fluor™ 488-conjugated isotype-matched anti-IgG (H+L) or isotype-matched anti-IgM (H+L) antibody (1:200; Invitrogen, Carlsbad, CA) in FACS buffer on ice for 45 min. The cells were then resuspended in 400 μl of FACS buffer containing propidium iodide (PI). Cell surface protein was detected by the flow cytometer FC500 and data was analyzed by FlowJo Ver.10. Different of mean fluorescent intensity (Diff.M.F.I) values was obtained by subtracting CALR, ERp57, HSP90, HSP70, ANXA1 or F-actin staining with respective IgG staining by FlowJo Ver.10. For immunofluorescence detection of CALR and F-actin, cells cultured in chamber slide were fixed with 4% paraformaldehyde at room temperature for 15 min, followed by blocking with FASC buffer and incubated with anti-CALR (1:100; Abcam) or anti-F-actin (1:100, Abcam) antibody at 4 ºC overnight. After washing, the cells were incubated with Alexa Fluor™ 488-conjugated isotype-matched anti-IgG (H+L) (1:200, Invitrogen) or isotype-matched anti-IgM

(H+L) antibody (1:200; Invitrogen) in FACS buffer at room temperature for 45 min followed by DAPI staining. The labeled cells were then examined by fluorescence microscopy.

ATP and HMGB1 assays. Extracellular ATP levels in conditioned medium and intracellular ATP levels in cell lysate followed the indicated treatment were measured by a luciferin-based ENLITEN ATP assay kit (Promega, Madison, WI) and an ATP assay kit (Merck, Darmstadt, Germany) according to the manufacturer's instruction respectively. HMGB1 concentrations in the conditioned medium followed the indicated treatment were measured by an HMGB1 ELISA kit (Shino-Test Corporation, Tokyo, Japan) according to the manufacturer's instruction. Luminescence and absorbance were measured using Perkin Elmer 2030 Multiable Reader VICTOR X4 (PerkinElmer, Waltham, MA) and Uquant MQX200 microplate reader spectrophotometer (Bio-Tek, Winooski, Vermont) respectively.

Quantitative real-time RT-PCR. Total RNA was extracted using TRIzol Reagent (Invitrogen) and transcribed into cDNA using a High Capacity cDNA kit (Applied Biosystems, Foster City, CA) according to the manufacturer's protocol. Real-time quantitative reverse transcription–PCR (qRT-PCR) was performed with TaqMan probes for Ccl2, Cxcl10, Ifnb1, Nfkbiz, Tlr4 or Actb (all from Applied Biosystems) using an ABI Prism 7900HT Sequence Detection System (Applied Biosystems). Relative mRNA gene expression was calculated using a $2^{-\Delta Ct}$ method (Applied Biosystems User Bulletin N°2, P/N 4303859).

Cytoplasmic and nuclear fractionation. Cells from 100 mm culture plate were trypsinized and resuspended in complete culture medium after the indicated treatment. Cell pellet was collected by centrifugation at 1000 rpm at 4 °C and then subject to cytoplasmic and nuclear protein fractionation by NE-PER^{TM} Nuclear and Cytoplasmic Extraction Reagent (Pierce

Biotechnology, Rockford, IL) according to the manufacturer's protocol. Protein concentration was measured by a Pierce™ BCA Protein Assay Kit (Pierce Biotechnology). The cytoplasmic and nuclear protein were stored at -80 °C prior to Western blot analysis.

Phos-tag SDS-PAGE. Detection of SNAP23 phosphorylation was done by Phos-tag SDS-PAGE as mentioned previously (21). Briefly, total cell lysates were extracted using RIPA buffer (Pierce Biotechnology, Rockford, IL). One microgram of extracted protein from each sample was used in Phos-tag SDS-PAGE (7.5% polyacrylamine gels containing 50 μM Phos-tag acrylamine and 100 μM $MnCl_2$ (Wako Pure Chemical Industries, Ltd., Osaka, Japan)). After electrophoresis, the Phos-tag acrylamine gels were washed with transfer buffer (50 mM Tris, 384 mM glycine, 0.1% SDS, 20% methanol) containing 1 mM EDTA for 10 min with gentle shaking prior to Western blot analysis.

Western blot analysis. Total cell lysates were extracted using RIPA buffer and 10 μg of extracted protein were used for Western blot. Specific primary antibodies were applied to probe the target proteins, including anti-HMGB1 (1:2000; Cell Signaling Technology), anti-PERK (1: 2000; Cell Signaling Technology), anti-eIF2α (1:2000; Cell Signaling Technology), anti-phospho-eIF2α (Ser51; 1:2000; Cell Signaling Technology), anti-TLR4 (1:2000; Cell Signaling Technology), anti-IKKβ (1:2000; Cell Signaling Technology), anti-phospho-IKKβ (1:2000; Cell Signaling Technology), anti-p105/p50 (1:2000; Cell Signaling Technology), anti-p65 (1:2000; Cell Signaling Technology), anti-RelB (1:2000; Cell Signaling Technology), anti-SNAP23 (1:2000; Abcam), anti-F-actin (1:2000; Abcam) and anti-β-actin (1:10000; Sigma-Aldrich). After probing with an HRP-linked secondary antibody (1:2000, GE Healthcare, Chicago, IL), the signals were detected with ECL Reagent (PerkinElmer).

ATP-containing vesicles staining. ATP-containing vesicles was detected using quinacrine staining (22). Briefly, cells were cultured in 8-well chamber slides 1 x 10^4 (per well) Nalge Nunc International, Naperville, IL) for 24 hr. After indicated treatment, the cells were washed with PBS and fixed with 4% paraformaldehyde, followed by incubated with 5 μM quinacrine (Sigma-Aldrich) for 30 min to label ATP-containing vesicles. The cells were then washed with PBS and examined by fluorescence microscopy.

***In vivo* model of tumor vaccination assay.** All mice were maintained in pathogen-free conditions and the *in vivo* experiments were performed according to (23) under the guidelines of The Chinese University of Hong Kong Animal Experimentation Ethics Committee. Briefly, ID8F3 cells (wild type or TLR4 KO) were incubated with paclitaxel (20 μM) for 48 hours, and those treated with DMSO were served as control groups. After drug treatments, the cells were harvested and resuspended in PBS at a concentration of 1 x 10^7 cells/ml. For vaccination, 50 μl of the resuspended cells (5 x 10^5 cells per mouse) was injected subcutaneously (s.c.) to the left flank of immunocompetent C57BL/6 mice (8-week-old female; n=5 per group). After 7 days, the vaccinated mice were re-challenged with live untreated wild type ID8F3 cells (5 x 10^6 cells per mouse) by intraperitoneal (i.p.) injection. Tumor growth was monitored regularly for the following weeks; the experiment would be stopped as soon as the mice become unmanageable (duration averaged about 50-60 days), i.e. with the development of ascitic fluid that caused movement problems or when the weight of the mouse became over 30 g. The absence of ascitic fluid developed in the mice after 120-day post i.p. injection was considered as an indication of absence of tumor and thus efficient antitumor vaccinations. All mice were eventually sacrificed for examination to confirm the absence or presence of peritoneal tumor development. The experiment was repeated twice.

Microarray gene expression data analysis. The microarray gene expression data (Accession no. GSE15622; including data from 20 ovarian cancer patients randomized to paclitaxel monotherapy in CTCR-OV01) from Gene Expression Omnibus (GEO) database (24) was adopted. For immune cell profiling analysis, data of the 14 patients whom had a matched biopsy performed before and after 3 cycles of paclitaxel monotherapy (with 11 patients responded and 3 patients resistant to the chemotherapy) were selected. The immune cell type of each sample was inferred using gene expression enrichment analysis by xCell pipeline (a novel gene signature-based method; http://xCell.ucsf.edu/; (25)), and the levels of each immune cells type were represented as enrichment scores (ES). Differential expression of immune cell types was determined by comparing the ES between pre- and post-chemotherapy samples using DChip analysis (DChip; http://www.dchip.org). Correlations between the mRNA expression level of TLR4 and ES of immune cells types in post-chemotherapy samples of 11 patients who responded to the chemotherapy were determined by Pearson correlation analysis. In addition, gene expression levels of CALR in the biopsies (pre-paclitaxel monotherapy) from patients responded (n=13) and resistant (n=7) to the chemotherapy were extracted from the database and analyzed by Mann-Whitney U test.

Immunohistochemistry and image analysis of TLR4 and CALR. Sections of 4 μm thickness from formalin-fixed paraffin-embedded ovarian tumor specimens were prepared. The slides were deparaffinized, rehydrated in graded ethanol, and fixed in neutral buffered formalin. Protein expression of TLR4 in ovarian tumor tissues were examined by routine IHC (26) using TLR4-specific antibody (1:25; R&D Systems, Minneapolis, MN). Protein expression of CALR was detected by IHC using a Ventana BenchMark XT system (a fully automated IHC slide staining instrument; Roche, Basel, Switzerland). In brief, after deparaffinization and rehydration, paraffin-embedded tissue sections were subject to Ventana

BenchMark XT platform. Sections were blocked with 3% hydrogen peroxide at room temperature for 4 min, and then treated with heat-induced antigen retrieval CC1 (Cell Conditioning 1; Roche) solution using the optimized antigen retrial condition, followed by incubating with CALR-specific antibody (1:500; Abcam) at 37 °C for 30 min. Then the tissue sections were incubated with OptiView HRP Linker for 12 min and OptiView HRP multimer for 12 min, and finally developed with 3,3′-diaminobenziding (DAB) for 4 min. Nuclei were then counterstained with hematoxylin.

Images at 200x fields were captured by Mantra™ Quantitative Pathology Workstation (PerkinElmer) using a brightfield protocol. Ovarian tumour tissues stained with hematoxylin or DAB alone were prepared to develop a spectral library that contains the spectral peaks of individual dyes for spectral unmixing and identification of signals using the inForm® 2.4.2 image analysis software (PerkinElmer). All spectrally unmixed images were subject to a trainable tissue segmentation tool of the inForm software that distinguishes tumoral area from stromal and blank areas. A cell segmentation tool was subsequently applied to classify the associated cellular compartments (nuclei, cytoplasm for TLR4, and membrane for CALR) in the segmented tumoral areas based on an object-based approach, in which hematoxylin was selected for nuclear segmentation, while cytoplasm and membrane were selected as the cellular compartments for pixel validation of TLR4 and CALR respectively. Protein expression in tumoral areas were scored from 0 to 3+ to bin spectrally unmixed signals into 4 bins. H-score for each image was computed by the software using the percentages in each bin that ranges from 0-300.

Opal™ multiplex IHC and multispectral imaging analysis of CD8, CD208, and IFN-γ.

Sections of 4 μm thickness were prepared as above. Antigen retrieval was performed using AR6 Buffer (PerkinElmer) and peroxidase activity was blocked by Dako REAL™ Peroxidase-Blocking Solution (Agilent, Santa Clara, CA). Opal multiplexed assay was carried out with each section subject to 3 successive rounds of antibody staining, each of which consists of 1) protein blocking, 2) incubation with primary antibodies: CD8 (1:25, Abcam), CD208 (1:250, Dendritics, Dardilly, France) and IFN-γ (1:500, Santa Cruz Biotechnology) were stained sequentially; 3) incubation with HRP-conjugated secondary antibodies: Opal Polymer HRP Ms + Rb (PerkinElmer) was applied to the primary antibody against CD8 and IFN-γ, while Rabbit Anti-Rat IgG H&L (HRP) (Abcam) was applied to the primary antibody against CD208; 4) tyramide signal amplification (TSA)-conjugated fluorophore. CD8, CD208 and IFN-γ were visualized using Opal 520 (1:50), Opal 570 (1:150) and Opal 690 (1:100) respectively. Microwave treatment in AR6 Buffer was repeated before next round of staining to remove the bound antibody being detected by the TSA reagent. After incubation with the last antibody, nuclei were counterstained with DAPI (Perkin Elmer) and mounted with ProLong™ Diamond Antifade Mountant (Invitrogen). Tumor tissue without primary antibodies was served as negative controls.

The positively labeled CD8+ T cells, CD208+ dendritic cells and IFNγ+ cells in the specimens were then quantified. All five filter cubes in the Mantra™ Quantitative Pathology Workstation associated with spectral bands for DAPI, FITC, CY3, Texas Red, and CY5 were employed for multispectral imaging. One 200x representative image of each marker that emits single or multiple spectral bands was selected to set the exposure times for image acquisition. Spectral unmixing was performed using the inForm® 2.4.2 image analysis software with a spectral library containing spectral peak information of all fluorophores. Images from the negative control slide was acquired to assess the autofluorescence signal. All

spectrally unmixed images were subject to the trainable tissue segmentation tool of the inForm software that distinguishes the tissue areas of interest from necrotic or blank areas, followed by the cell segmentation tool that classifies the associated cellular compartments (nuclei, cytoplasm and membrane) in the segmented tissue areas based on a DAPI counterstain-based approach. The cell phenotyping recognition learning algorithm tool was then applied to identify the cells positively stained for individual markers. Tissue area and cell counts in the segmented areas in each image were quantitated for the evaluation of cell density for each tumor specimen. Cell density (in megapixel) per 200x field image was accounted by the number of cells per tissue area.

Statistical analysis. All data was described as mean ± S.E.M. and analyzed using GraphPad Prism 5.0 software (GraphPad Inc., San Diego, CA, USA) from at least three independent experiments. Statistical difference between experimental groups was determined by Student's t test and Mann-Whitney U test. Correlation between experimental groups was determined by Pearson correlation. Survival analysis was performed by the Kapan-Meier curves and log-rank test were generated using GraphPad Prism 5.0 software. Chi-Square $\chi 2$ test was performed by SPSS version 18.0 software. $p < 0.05$ were considered as statistically significant (*), $p < 0.01$ as highly significant (**) and $p < 0.001$ as extremely significant (***).

Results

Paclitaxel, but not carboplatin, induces immunogenic cell death in syngeneic murine models of ovarian tumor

We investigated if the standard-of-care chemotherapeutic drugs, including carboplatin and paclitaxel, induce ICD in ovarian cancer by examining the associated DAMPs in ID8 murine-derived ovarian cancer cell line (6, 27). Mitoxantrone being a well-known inducer of ICD was used as positive controls (7, 28). Cisplatin, on the other hand, was used as negative controls as it is incapable of eliciting CALR translocation from the lumen of ER to cell surface and thus fails to induce ICD in syngeneic murine model of colon cancer (29) (see also Fig. 4A and Supplementary Fig. S4F). We first treated ID8 murine ovarian cancer cells with serial dilutions (0.1 μM to 1000 μM) of paclitaxel, cisplatin, carboplatin or mitoxantrone for 48 hours, and determined their half maximal inhibitory concentrations (IC50) by growth inhibitory assays as follows: 20 μM (paclitaxel), 200 μM (carboplatin) and 1 μM (mitoxantrone). The IC50 of each drug was confirmed by flow cytometry with cells double-stained with annexin V (AnnV) and propidium iodide (PI), which showed more than 70% of cell death (AnnV+PI- represents apoptotic cell death, AnnV+PI+ represents necrotic cell death and AnnV-PI+ represents non-apoptotic cell death) individually (Fig. 1A) and was applied to the following experiments unless otherwise specified. Nevertheless, we applied cisplatin at a lower concentration of 300 μM instead of a high level of IC50 for cisplatin (500 μM) in order to limit the concentration of its solvent i.e. DMSO to 3%.

We then examined the surface expressions of CALR and ERp57 on dying (but not dead) ID8 cells after drug treatments by flow cytometry (8). Our results showed that paclitaxel and mitoxantrone, but not carboplatin and cisplatin, induce an increase in CALR and ERp57 exposure on the cell surface membrane of dying ID8 cells (Fig. 1B and

Supplementary Fig. S1A). We also examined the ATP levels in the conditioned media of ID8 cells by luciferin-based ENLITEN ATP assay, and found high levels of extracellular ATP in ID8 cells treated with paclitaxel and mitoxantrone, while a significantly low level of intracellular ATP was found in ID8 cells treated with mitoxantrone (Fig. 1C). Besides, both our ELISA and Western blot analyses demonstrated high levels of HMGB1 in the conditioned media of ID8 cells after the treatment with paclitaxel, carboplatin or mitoxantrone (Fig. 1D). We also found that among the drugs only paclitaxel induces an increase in ANXA1 exposure in dying ID8 cells (Fig. 1E and Supplementary Fig. S1A). Paclitaxel was also shown to induce Cxcl10 upregulation (Fig. 1H). On the other hand, surface exposure of heat shock proteins (HSP70 and HSP90) was found in anthracyclines-treated human tumor cells (9). We could not, however, detect any significant increase in the surface expression of HSP70 and HSP90 in dying ID8 cells treated with paclitaxel or carboplatin (Fig. 1F, G and Supplementary Fig. S1A). Treatments with paclitaxel or carboplatin also posed no significant effect on the upregulation of type I IFNs (Ifnb1) (Fig. 1H). These results demonstrated that paclitaxel, but not carboplatin, induces the release of multiple ICD-associated DAMPs, including CALR and ERp57 exposure, ATP secretion, HMGB1 release, AXNA1 exposure and Cxcl10 upregulation in ID8 murine ovarian cancer cells *in vitro*. Additionally, similar observations on paclitaxel inducing multiple DAMPs were found in two other murine ovarian cancer cell lines including TKO (Supplementary Fig. S1B-G) and ID8F3 cells (Supplementary Fig. S1H-L).

We then performed *in vivo* assessments of the above observations on DAMPs by "tumor vaccination" assays in order to validate the paclitaxel-induced ICD in syngeneic model (23). In brief, after exposing the murine-derived tumor cell line ID8F3 with paclitaxel (20 μM) *in vitro*, we injected the tumor cells subcutaneously into one flank of

immunocompetent mice. After a latency of one week, the mice were re-challenged with live non-treated tumor cells of the same type intraperitoneally. Tumor incidence and growth were routinely monitored; the proportion of mice that does not develop tumors reflects the degree of ICD-mediated antitumor response induced by drug treatment (4, 30). Our result demonstrated a significant increase in tumor-free survival among mice immunized with paclitaxel-treated ID8F3 murine ovarian tumor cells when compared to the controls (immunized with DMSO-treated ID8F3 tumor cells) (Fig. 1I), thus indicating paclitaxel is a *bona fide* inducer of ICD that turns tumor cells into tumor vaccines in the syngeneic mouse model of ovarian cancer.

The role of paclitaxel in antitumor activity has long been recognized by stabilizing microtubules that results in mitotic cell death and G2/M phase cell cycle arrest (31-33). We therefore set up a time-course experiment (0-48 hours) to study the correlation between paclitaxel-induced cell death/cell cycle arrest and paclitaxel-induced DAMPs in ID8 murine ovarian cancer cells. Our results indicated that paclitaxel induces cell death (AnnV+PI- cells, AnnV+PI+ cells and AnnV-PI+ cells) and G2/M phase arrest from 24-48 hours post-treatment (Supplementary Fig. S2A). Moreover, significant increases were observed in the CALR and ERp57 exposure, levels of ATP secretion and HMGB1 release, ANXA1 exposure and Cxcl10 upregulation (Supplementary Fig. S2B-F) after paclitaxel treatment for 24-48 hours, indicating the paclitaxel induced DAMPs is correlated with the cell death and mitotic arrest mediated by paclitaxel.

Paclitaxel requires cancer cell-autonomous TLR4 to induce immunogenic cell death in murine ovarian tumor

Next, we sought to explore the molecular mechanism underlying the paclitaxel-induced ICD in our syngeneic mouse models of ovarian cancer. We investigated the role of an innate immune receptor for paclitaxel, TLR4 (34-36), on the surface of ovarian cancer cells by generating isogenic derivatives of ID8 and ID8F3 cells that lack Tlr4 expression (*Tlr4-/-*) with CRISPR-Cas9. High levels of endogenous TLR4 in wild type ID8 and ID8F3 cells were demonstrated by qRT-PCR and Western blot analyses, together with the absence of Tlr4 gene transcription and protein expression in our isogenic derivatives of ID8 (Tlr4 KO 3F, 8A, 8H, 10G and 11F) and ID8F3 (Tlr4 KO 1A1) Tlr4 knockout (KO) clones (Supplementary Fig. S3A). We did not observe any significant difference in cell proliferation or endogenous cytokine expression (Ccl2 and Cxcl10) (Supplementary Fig. S3B, C) nor in paclitaxel-induced cell death and G2/M phase arrest (Supplementary Fig. S3D, E) between the wild type and Tlr4 KO clones. These data thus indicated the absence of TLR4 does not affect the cell proliferation and endogenous cytokine expression of ovarian cancer cells, while the paclitaxel-induced cell death and mitotic arrest are also TLR4 independent.

We then investigated the immunogenicity of cell death induced by paclitaxel in the ID8 Tlr4 KO clones, and found reduced levels of the ICD-associated DAMPs including CALR and ERp57 exposure, ATP secretion, HMGB1 release, ANXA1 exposure and Cxcl10 expression when compared to the wild type ID8 cells (Fig. 2A-E and Supplementary Fig. S3F). Nevertheless, the levels of mitoxantrone-induced DAMPs in the KO clones have no significant difference when compared with the wild type (Supplementary Fig. S3G, H). In addition to the gene knockout studies, we have also inhibited the endogenous TLR4 activity of wild type ID8 cells by its antagonist TAK-242 (37). The pre-treatment of TAK-242 also showed reduced levels of paclitaxel-induced CALR and ERp57 exposure, ATP secretion, HMGB1 release, ANXA1 exposure and Cxcl10 expression (Fig. 2F-J and Supplementary Fig.

S3I). Our *in vivo* tumor vaccination assays confirmed these findings by showing no significant difference in tumor-free survival of the mice immunized with paclitaxel-treated *Tlr4-/-* ID8F3 cells when compared with controls (DMSO-treated *Tlr4-/-* ID8F3 cells) (Fig. 2K). These results thus indicated paclitaxel requires cancer cell-autonomous TLR4 to induce ICD-associated DAMPs that converts tumor cells into tumor vaccines in murine ovarian cancer.

Paclitaxel activates canonical NF-κB signaling pathway in murine ovarian cancer cells via TLR4/MyD88-dependent pathway

Since the above data indicated the paclitaxel-induced ICD requires cell-autonomous TLR4 in ovarian cancer, we investigated if the MyD88-dependent TLR4 signaling pathway, which activates canonical NF-κB (nuclear factor-κB) signaling (38), is involved. Here we confirmed two major adaptors that bind to the intracellular domain of TLR4, MyD88 and TRIF (TIR (toll/inerleukin-1 receptor)-domain-containing adapter-inducing interferon-β) (39), are expressed in wild type ID8 murine cells (Fig. 3A and Supplementary Fig. S4A). Besides, our Western blot analyses with nuclear and cytoplasmic extraction showed that paclitaxel induces nuclear translocation of NF-κB p50 and p65 subunits in the ID8 cells (Fig. 3B and Supplementary Fig. S4B). The paclitaxel-induced NF-κB activation (i.e. nuclear translocation of p65) was diminished in the ID8 Tlr4 KO clones as well as in TAK-242-treated wild type ID8 cells (Fig. 3C, D and Supplementary Fig. S4 C, D). These results indicated that paclitaxel induces the activation of canonical NF-κB signaling in murine ovarian cancer cells via TLR4/MyD88-dependent pathway.

Paclitaxel induces Ccl2 transcription in murine ovarian cancer cells via TLR4/MyD88/NF-κB signaling pathway

Chemokine CCL2/chemokine receptor CCR2 signaling axis was shown to be essential for the recruitment of functional antigen-presenting cells into tumor bed upon anthracycline-based chemotherapy (40). Here we investigated if CCL2 is involved in the paclitaxel-induced ICD which elicits antitumor immunity driven by intratumoral dendritic cells. We first demonstrated that paclitaxel (but not carboplatin, cisplatin or mitoxantrone) induces upregulation of Ccl2 mRNA expression in ID8 cells (Fig. 3E). The levels of paclitaxel-induced Ccl2 upregulation were reduced in the ID8 Tlr4 KO clones (Fig. 3F), and also in wild type ID8 cells with the pre-treatment of Tlr4-specific siRNA (Fig. 3G) or TAK-242 (Fig. 3H), thus indicating paclitaxel induces Ccl2 upregulation in murine ovarian cancer cells that depends on TLR4 signaling.

We also investigated the role of a transcriptional key regulator of CCL2, namely IκBζ (Nfkbiz, nuclear factor of kappa light polypeptide gene enhancer in B-cells inhibitor zeta) in paclitaxel-induced Ccl2 transcription in ovarian cancer cells (41). The transcription of IκBζ is regulated by TLR4/MyD88/NFκB pathway, which forms a complex with p50 and p65 on the promoter of target genes and activates their expression (42). Our results showed that paclitaxel induces significant upregulation of Nfkbiz mRNA in wild type ID8 cells (Fig. 3I), but the levels of upregulation were reduced in the ID8 Tlr4 KO clones (Fig. 3J) and in wild type ID8 cells with the pre-treatment of Tlr4-specific siRNA (Fig. 3K) or TAK-242 (Fig. 3L), indicating the paclitaxel-induced Nfkbiz upregulation in murine ovarian cancer cells is dependent on TLR4. We studied further by blocking the NF-κB p65 activation of wild type ID8 cells with an inhibitor BAY 11-7082 (Fig. 3M and Supplementary Fig. S4E), and showed that the pre-treatment of BAY 11-7082 suppresses the paclitaxel-induced Nfkbiz,

Ccl2 mRNA transcription (Fig. 3N) and Ccl2 promoter activity (Fig. 3O). Our results thus indicated paclitaxel induces Ccl2 transcription in murine ovarian cancer cells via TLR4/NFκB signaling pathway.

Paclitaxel induces PERK activation and eIF2α phosphorylation in murine ovarian cancer cells via a TLR4-independent manner

Besides, we also investigated the upstream signaling pathway of CALR and ERp57 exposure in the paclitaxel-induced ICD. Previous studies revealed that CALR exposure is reliant on responses to several immunogenic chemotherapeutic agents via ER stress that triggers PERK (protein kinase R-like ER kinase) activation and eIF2α (eukaryotic translation initiation factor 2α) phosphorylation (4, 28). Here our Western blot analyses showed that paclitaxel and mitoxantrone, but not carboplatin and cisplatin, induce PERK activation by a mobility shift with anti-PERK antibodies and eIF2α phosphorylation using antibody specific to eIF2α phosphorylation on serine 51 (43, 44) in both ID8 and TKO murine ovarian cancer cell lines (Fig. 4A-C and Supplementary Fig. S4F-H). We also found that both paclitaxel and mitoxantrone induce PERK activation and eIF2α phosphorylation in the ID8 Tlr4 KO clones when compared with wild type ID8 cells (Fig. 4D, E and Supplementary Fig S4I, J). Additionally, the pre-treatment with TAK-242 that inhibits TLR4 activities did not affect the levels of paclitaxel-induced PERK activation and eIF2α phosphorylation in the ID8 cells (Fig. 4F and Supplementary Fig. S4K). Our results therefore indicated paclitaxel induces PERK activation and eIF2α phosphorylation in murine ovarian cancer cells independent of TLR4.

Paclitaxel induces SNARE-dependent exocytosis of ATP-containing vesicles in murine ovarian cancer cells via TLR4-mediated IKK2 activation

We have demonstrated that in the absence of TLR4, paclitaxel is able to induce ER stress (PERK activation and eIF2α phosphorylation; Fig. 4D) but not CALR exposure (Fig. 2A) in murine ovarian cancer cells. Here we studied further the mechanism underlying CALR exposure based on the "translocation module", which involves the anterograde transport of CALR by actin cytoskeleton from ER to Golgi apparatus, followed by active exocytosis of CALR-containing vesicles to plasma membrane surface via molecular interactions between vesicle-associated SNAREs (soluble *N*-ethylmaleimide-sensitive factor attachment protein receptors, such as VAMP1) and plasma membrane-associated SNAREs (such as SNAP23/25) (4, 45, 46). The mechanism to which actin cytoskeleton mediates the anterograde transport of CALR during anthracycline treatment remains poorly understood. Here we showed F-actin is exposed to the cell surface of ID8 wild type cells treated with paclitaxel or mitoxantrone (Supplementary Fig. S5A, B). The levels of paclitaxel-induced F-actin exposure were reduced in the ID8 Tlr4 KO clones (Supplementary Fig. S5C), suggesting paclitaxel induces the actin-cytoskeleton-mediated anterograde transport of CALR from ER to Golgi via TLR4-dependent pathway.

We continued our study on the role of paclitaxel-induced SNARE-dependent vesicle exocytosis in murine ovarian cancer cells via IkappaB kinase 2 (IKK2) activation. It has been reported that SNARE-dependent vesicle exocytosis is the final step of CALR exposure to the cell surface, in which depletion of the plasma membrane-associated SNARE, namely SNAP23, abolished the anthracycline-induced ICD in mouse colon tumor (4, 28). Studies also showed that TLR/MyD88 signaling pathway transduces the IKK2-mediated phosphorylation of SNAP23 in dendritic cells (47), and leads to mast cell degranulation and

controls platelet secretion (48, 49). Here our results demonstrated that paclitaxel induces IKK2 phosphorylation in the wild type ID8 cells (Fig. 5A and Supplementary Fig. S5D), but the phosphorylation was diminished in the Tlr4 KO clones and the TAK-242-treated wild type ID8 cells (Fig. 5B, C and Supplementary Fig. S5E, F), indicating that paclitaxel induces IKK2 activation in ovarian cancer cells via TLR4/MyD88 signaling. We also demonstrated paclitaxel induces SNAP23 phosphorylation in wild type (Fig. 5D and Supplementary Fig. S5G) but not in the ID8 Tlr4 KO clones or TAK-242-treated wild-type ID8 cells (Fig. 5E, F and Supplementary Fig. S5H, I) by Phos-taq SDS-PAGE (for the separation of phosphorylated substances) with an anti-SNAP23 antibody. We then blocked the IKK2 phosphorylation by treating the ID8 cells with inhibitors TPCA-1 and IKK2 inhibitor IV. Our results showed that TPCA-1, but not IKK2 inhibitor IV, inhibits the paclitaxel-induced IKK2 phosphorylation in ID8 cells (Fig. 5G and Supplementary Fig. S5J). Our results also showed that the paclitaxel-induced SNAP23 phosphorylation was reduced in the TPCA-1-treated wild-type ID8 cells (Fig. 5H and Supplementary Fig. S5K). These results indicated that paclitaxel induces IKK2-mediated phosphorylation of SNAP23 in murine ovarian cancer cells via TLR4 pathway. Furthermore, the levels of paclitaxel-induced CALR, ERp57 and ANXA1 exposure were also reduced in the wild type ID8 cells pre-treated with of TPCA-1 (Fig. 5I and Supplementary Fig. S5L), suggesting IKK2-mediated SNAP23 phosphorylation plays a key role in the ICD-associated DAMPs induced by paclitaxel.

Next we studied the effect of paclitaxel on vesicle exocytosis in ovarian cancer cells by monitoring ATP-containing vesicles using quinacrine staining (22) as it is difficult to visualize the active status of vesicle exocytosis. Our results showed that paclitaxel induces quinacrine-positive ATP-containing vesicles in the wild type ID8 cells, suggesting paclitaxel induces ATP synthesis for secretion (Fig. 5J). A substantially higher number of ATP-

containing vesicles induced by paclitaxel was observed in the Tlr4 KO clones as well as in the TAK-242 or TPCA-1-treated wild type ID8 cells (Fig. 5J, K). The increase in the number of ATP-containing vesicles may be correlated with the reduced activities in SNARE-dependent vesicle exocytosis associated with the absence of TLR4 activities (Fig. 5E, F) or IKK2 phosphorylation (Fig. 5H) and thus retains the ATP inside the cell. These results indicated that paclitaxel induces SNARE-dependent vesicle exocytosis in ovarian cancer cells via TLR4-mediated IKK2 activation.

Paclitaxel chemotherapy induces immunology cell death and antitumor immune response in human ovarian cancer

We pursued our study further on the paclitaxel-induced ICD that elicits antitumor responses in human ovarian cancer. A previous study has demonstrated that anthracyclines are able to induce the expression of several ICD-associated DAMPs as well as antitumor immunity in human primary tumors and cell lines of ovarian cancer (9). Here we found that in human ovarian cancer cell lines SKOV3, paclitaxel induces CALR and ERp57 exposure, ATP secretion and HMGB1 release *in vitro* (Fig. 6A and Supplementary Fig. S5M). We also investigated the immune cell profiling of ovarian tumor microenvironment from the advanced ovarian cancer biopsy expression dataset GSE15622 that contains both responsive and resistant cases to paclitaxel monotherapy (24). In the GSE15622 dataset, there were 14 patients (out of 20) with ovarian cancer who had a biopsy performed before and after 3 cycles of paclitaxel monotherapy. We have analyzed 33 immune cell types in these 14 cases by gene expression enrichment analysis using xCell pipeline (a novel gene signature-based method) (25) in pre- and post-paclitaxel monotherapy samples, and found that the enrichment scores (ES) of various types of T cell, including CD4+ memory T cells, CD8+ Tcm cells, CD4+ T

cells, CD8+ T cells, and CD4+ naïve T cells, were significantly higher in post-treatment than in the pre-treatment samples of responsive patients. Such differences in T cell induction were not observed between the post- and pre-treatment samples of resistant patients (Fig. 6B). Apart from the publicly available gene expression microarray dataset, we have also analyzed T cell infiltration in 9 cases of advanced ovarian tumors from patients receiving NACT (neoadjuvant chemotherapy; 8 cases with paclitaxel-carboplatin regimen and 1 case with carboplatin monotherapy) followed by interval debulking surgery and 9 cases of high grade serous ovarian cancer (HGSOC) from patient receiving primary debulking surgery (at Department of Obstetrics and Gynaecology, The Chinese University of Hong Kong, Prince of Wales Hospital) by multiple immunohistochemistry (mIHC). Our results showed that the number of CD8+ T cells, IFNγ+ cells and IFNγ+CD8+ T cells were significantly higher in post-NACT ovarian tumors than those in primary ovarian tumors (Fig. 6C and Supplementary Fig. S6A-C). On the other hand, the number of positively labeled infiltrating CD8+ T cells, IFNγ+ cells and IFNγ+CD8+ T cells was comparatively smaller in the ovarian tumor of patients with carboplatin monotherapy (Fig. 6C and Supplementary Fig. S6A-C) than those with combinatorial therapy. These data suggested that paclitaxel chemotherapy induces T cell infiltration in ovarian tumors of the responsive patients.

We then tested if the T cell infiltration after paclitaxel chemotherapy is correlated with TLR4 expression in ovarian cancer. In the post-paclitaxel monotherapy samples of responsive patients (n=11; GSE15622), significantly positive correlations between TLR4 mRNA expression and T cell gene expression enrichment scores (including CD8+ T cells, CD8+ Tem cells, CD4+ Tem cells, CD8+ Tcm cells and CD4+ naïve T cells) were found (Fig. 6D), thus indicating high levels of TLR4 expression in ovarian tumor favors higher amount of T cell infiltration after paclitaxel chemotherapy. Next, we studied the prognostic

impact of TLR4 and CALR expression in ovarian cancer by immunohistochemistry (IHC) in the tumor samples of 124 patients with epithelial ovarian cancer (EOC; including 45 high grade serous, 42 clear cell, 22 endometroid, 13 mucinous, 1 adenocarinoma and 1 mixed serous and clear cell (Supplementary Table S1)) who received primary debulking surgery. Positive signals of TLR4 expression in the cytoplasm and CALR expression on the surface membrane of ovarian epithelial tumor cells were evaluated by H-score using an imaging software inForm, in which patients with EOC were divided into three groups based on their expression levels of TLR4 cytoplasmic expression and CALR surface expression according to their respective H-score (low: 0-33 percentile; medium: > 33-67 percentile; high: > 67-100; Supplementary Fig. S7A, B and S8A, B). Notably, our data showed that patients with high CALR surface expression have better overall survival and disease-free survival by Kaplan-Meier survival analyses (Fig. 6E), indicating CALR expressions in primary HGSOC tumors are correlated with patients' survival. These data also suggested that the paclitaxel-induced ICD (via CALR exposure) contributes to the chemotherapy treatment outcomes.

We studied further on the CALR expression in primary tumors from patients receiving paclitaxel chemotherapy. Among the pre-paclitaxel monotherapy samples from GSE15622 dataset, a significantly higher level of CALR mRNA expression was found in responsive patients when compared to those of resistant patients (Fig. 6F). Our IHC result also showed high CALR surface expression in primary EOC tumors are correlated with better responses to paclitaxel chemotherapy i.e. a significantly higher proportion of responsive patients were found among the group of patients with high levels of CALR surface expression in the EOC tumor cells (Fig. 6G). Our results therefore suggested that the paclitaxel-induced ICD-associated DAMPs is correlated with chemotherapy response.

Discussion

Paclitaxel, or taxol, was first put into clinical trials on patients with advanced ovarian cancer more than 30 years ago and has since become a widely used chemotherapeutic drug to treat patients with a variety of cancers, including those of the ovaries, breast and lung (33) (50). The action of paclitaxel has long been recognized in promoting microtubule polymerization and stabilization, which was believed to induce mitotic arrest in cancer therapy that leads to cell death in a subset of the arrested population at concentrations similar to those in cell culture and animal tumor models (31, 51). Recent evidence, however, demonstrates that the intratumoral concentrations of paclitaxel in primary breast tumor specimens are too low to cause mitotic arrest but would result in multipolar divisions instead (33, 50). The present study reveals the capability of paclitaxel to induce the immunogenicity of dying tumor cells that elicits antitumor immune response in ovarian cancer which correlates with better survival. It also provides insights into understanding why a significant proportion of patients with advanced ovarian cancer (70-80%) receiving standard treatments, i.e. debulking surgery and chemotherapy, attained complete responses initially. Our findings of paclitaxel-induced ICD and hence antitumor effect in ovarian cancer, which highlights the importance of CALR expression as indicator, will not only benefit to the patients with the disease, but also to the those with breast and lung cancers.

In our study, we applied a concentration of paclitaxel (20 μM) that is routinely used to trigger cell death *in vitro* (52). We have to make sure the concentration of paclitaxel that we tested is high enough to induce more than 70% cell death in murine ovarian cancer cell lines for our *in vivo* tumor vaccination assays, which is a gold-standard experiment to validate ICD in syngeneic mice (7). We have also tested and confirmed that at lower concentrations (5 nM to 5 μM), paclitaxel were unable to induce a substantial number of cell death in the murine

ovarian cancer cells (Supplementary Fig. S1M, N). Furthermore, we showed here for the first-time that paclitaxel is able to induce multiple ICD-associated DAMPs, including CALR exposure, ATP secretion, HMGM1 release, ANXA1 exposure and CXCL10 upregulation in murine ovarian cancer cells *in vitro*. Our tumor vaccination assays validated the paclitaxel-induced ICD elicits antitumor immunity in murine model of ovarian tumor *in vivo*. A previous study on the drug treatment of U2OS human osteosarcoma cells with a chemical library that entails commonly used anti-neoplastic agents (including paclitaxel, 3μM) also reported that paclitaxel induces significant eIF2α phosphorylation, HMGB1 release and ATP secretion in the cell line (53). In addition, hyperploid cancer cells were shown to become immunogenic because of a constitutive ER stress response resulting in aberrant CALR surface exposure, and that the treatment of tetraploidizing agents (including 300 nM paclitaxel) induces CALR exposure in U2OS cells (54). Nevertheless, here we found that paclitaxel induces G2/M arrest and >4N (i.e. multinucleated) cell population in both the wild type ID8 cells and Tlr4 KO clones (Supplementary Fig. S3E), while we have already shown that the level of paclitaxel-induced CALR exposure was reduced in the Tlr4 KO clones (Fig 2A). These data thus suggest that tetraploidization does not correlate with the paclitaxel-induced ICD in in our murine ovarian cancer models.

The antitumor immunity induced by paclitaxel was demonstrated recently in modulating tumor-associated macrophages from a M2-like profile towards an immunocompetent M1-like phenotype via TLR4 signaling pathway in the murine models of breast and melanoma tumors (55). We demonstrated here that the cancer cell-autonomous TLR4 is essential in the paclitaxel induced CALR exposure in murine ovarian cancer cells based on our observations of a reduced paclitaxel-induced CALR exposure in Tlr4 KO clones. Literatures have revealed three different hierarchical modules of CALR exposure in response

to ICD inducers such as anthracyclines (45), including: 1) “ER stress module”, which involves eIF2α phosphorylation due to PERK activation (the kinase) or PP1/GADD34 inhibition (the phosphatase), ROS and/or NO production, and possible SERCA inhibition. Our study showed that paclitaxel induces PERK activation and eIF2α phosphorylation in the Tlr4 KO clones, indicating the paclitaxel-induced “ER stress module” of CALR exposure pathway is independent of TLR4; 2) “translocation module”, in which CALR is anterogradely transported from ER lumen to Golgi facilitated by actin cytoskeleton rearrangement, and the vesicle-associated SNARE (VAMP1) interacts with the plasma membrane-associated SNARE (SNAP23) and mediates membrane fusion by allowing luminal CALR to reach its final destination - the cell surface. We showed here that the paclitaxel-induced F-actin exposure in murine ovarian cancer cells is TLR4-dependent (Supplementary Fig. S5A-C), suggesting actin cytoskeleton-mediated the anterograde transport of CALR from ER to Golgi may involve in paclitaxel-induced CALR exposure via TLR4 signaling pathway. Besides, other studies have regarded F-actin as a DAMP recognized by DNGR-1 (also known as CLEC9A) (56-58), which is a dendritic cell receptor that couples sensing of necrosis to immunity (59). Our discovery of F-actin exposure in paclitaxel/mitoxantrone-induced ICD supports F-actin as a new ICD-associated DAMP in chemotherapy. In addition, we also showed paclitaxel induces IKK2 phosphorylation, SNAP23 phosphorylation, and ATP-containing vesicle exocytosis in wild type murine ovarian cancer cells, which levels of induction were reduced in the Tlr4 KO clones. These results indicated that paclitaxel induces the “translocation module” (i.e. SNARE-dependent vesicle exocytosis) of CALR exposure pathway via TLR4/IKK2 signaling; 3) “Apoptotic module”, which might mediate an inter-organellar crosstalk between the ER and mitochondria via apical caspase-8 dependent cleavage of Bap31 and activation of the Bcl-2 family proteins Bax and Bak, was however not investigated in the present study.

Our study demonstrated that paclitaxel induces ATP secretion in murine ovarian cancer cells via TLR4 signaling pathway. It is reported previously that autophagy is essential for the immunogenic ATP release from dying tumor cells (4, 60). In response to anthracycline chemotherapy, autophagy-competent cancers attracted dendritic cells and T lymphocytes into the tumor bed, whereas suppression of autophagy inhibited the release of ATP from the dying cells. Based on our study here with the conversion of LC3I to LC3II using Western blot, however, only a weak induction of autophagy could be detected in murine ovarian cancer cells after paclitaxel treatment when compared to that of the positive control using thapsigargin (Supplementary Fig. S1O). This indicated paclitaxel-induced ATP release in ovarian cancer cells does not depend on autophagy.

Whilst a previous study mainly focused on the capability of anthracyclines to induce ICD in human tumor cells, including CALR exposure, HSP70 and HSP90 secretion, and HMGB1 release (9), we showed here that paclitaxel also induces multiple ICD-associated DAMPs in human ovarian cancer cells *in vitro*. Furthermore, we have also investigated T cell infiltration (especially on CD8+ T cells) in human ovarian tumor beds after paclitaxel chemotherapy based on the recent evidence showing CD8+ T cell infiltration reflects antitumor immune response in ovarian tumors (61). NACT was associated with the increased densities of CD3+ and CD8+ TILs as revealed in an analysis on a large panel of immune cells in matched pre- and post NACT tumor samples from 26 HGSOC patients by IHC (62). Balkwill and colleagues also showed significant T cell activation, which involves enhanced IFNγ-producing CD4+ T cells and increased antitumor Th1 immune gene signatures, in omental biopsies from ovarian cancer patients after NACT when compared to those receiving primary debulking surgery (63). These data thus indicated paclitaxel chemotherapy induces T

cell infiltration i.e. antitumor immune response in ovarian tumor *in vivo*. Here we showed that paclitaxel chemotherapy induces T cell infiltration (including CD8+ T cells) in clinical samples of human ovarian tumors, which is associated with TLR4 expression in the tumor cells, and supports further that paclitaxel induces antitumor immune response in human ovarian tumor *in vivo*.

The study on anthracycline-induced ICD showed that CALR protein expression in human non-small cell lung cancers was correlated with an increased antitumor immune cell accumulation and favorable prognosis (64). In our study, we found that surface expression of CALR in primary HGSOC correlate with better prognosis. We also showed CALR surface expression correlates with patient's chemotherapy response. Our data suggests that paclitaxel-induced ICD associates with chemotherapy response and thus benefit the overall survival of patients with ovarian cancer.

In conclusion, our results demonstrated that paclitaxel induces ICD in ovarian cancer via TLR4-independent and TLR4-dependent pathways, including: 1) paclitaxel induces mitotic arrest, cell death as well as ER stress in a TLR4-independent manner; 2) paclitaxel induces Ccl2 (likewise Cxcl10) upregulation via TLR4/MyD88/NFκB pathways; and 3) paclitaxel induces SNARE-dependent vesicle exocytosis via TLR4-mediated IKK2 activation. The paclitaxel-mediated vesicle exocytosis is thought to be essential to the release of ICD-associated DAMPs (including CALR exposure, secretion of ATP, HMGB1, ANXA1 and CXCL10) in dying ovarian tumor cells (Fig. 7). Our results therefore provide new evidence that the antitumor effect of paclitaxel occurs in part via activation of antitumor immunity by inducing the immunogenicity of dying tumor cells, as well as insights into a new combination of paclitaxel and immunotherapies as an anticancer treatment for ovarian cancer.

Acknowledgements

The authors give special thanks to Prof. Samuel C. Mok, Department of Gynecologic Oncology and Reproductive Medicine, Division of Surgery, The University of Texas MD Anderson Cancer Center for the TKO cell line. The authors also give thanks to Dr. Amy Kit-Ying Chung for revising the manuscript.

Authors' contribution

TSL, and JK conceived experiments. TSL, LKYC, GCWM, ECHW, and JK carried out experiments. TSL, LKYC, and JK analysed data. JHSL, SFY, and THC collected clinical samples. IN offered the ID8F3 murine ovarian cancer cell line for some key experiments. All authors were involved in writing the paper and had final approval of the submitted and published versions.

References

1. Vaughan S, Coward JI, Bast RC, Jr., Berchuck A, Berek JS, Brenton JD, et al. Rethinking ovarian cancer: recommendations for improving outcomes. Nat Rev Cancer. 2011;11(10):719-25.

2. Coukos G, Tanyi J, Kandalaft LE. Opportunities in immunotherapy of ovarian cancer. Ann Oncol. 2016;27 Suppl 1:i11-i5.

3. Cristea M, Han E, Salmon L, Morgan RJ. Practical considerations in ovarian cancer chemotherapy. Ther Adv Med Oncol. 2010;2(3):175-87.

4. Kroemer G, Galluzzi L, Kepp O, Zitvogel L. Immunogenic cell death in cancer therapy. Annu Rev Immunol. 2013;31:51-72.

5. Green DR, Ferguson T, Zitvogel L, Kroemer G. Immunogenic and tolerogenic cell death. Nat Rev Immunol. 2009;9(5):353-63.

6. Galluzzi L, Buque A, Kepp O, Zitvogel L, Kroemer G. Immunogenic cell death in cancer and infectious disease. Nat Rev Immunol. 2017;17(2):97-111.

7. Obeid M, Tesniere A, Ghiringhelli F, Fimia GM, Apetoh L, Perfettini JL, et al. Calreticulin exposure dictates the immunogenicity of cancer cell death. Nat Med. 2007;13(1):54-61.

8. Panaretakis T, Joza N, Modjtahedi N, Tesniere A, Vitale I, Durchschlag M, et al. The co-translocation of ERp57 and calreticulin determines the immunogenicity of cell death. Cell Death Differ. 2008;15(9):1499-509.

9. Fucikova J, Kralikova P, Fialova A, Brtnicky T, Rob L, Bartunkova J, et al. Human tumor cells killed by anthracyclines induce a tumor-specific immune response. Cancer Res. 2011;71(14):4821-33.

10. Ghiringhelli F, Apetoh L, Tesniere A, Aymeric L, Ma Y, Ortiz C, et al. Activation of the NLRP3 inflammasome in dendritic cells induces IL-1beta-dependent adaptive immunity against tumors. Nat Med. 2009;15(10):1170-8.

11. Apetoh L, Ghiringhelli F, Tesniere A, Obeid M, Ortiz C, Criollo A, et al. Toll-like receptor 4-dependent contribution of the immune system to anticancer chemotherapy and radiotherapy. Nat Med. 2007;13(9):1050-9.

12. Vacchelli E, Ma Y, Baracco EE, Sistigu A, Enot DP, Pietrocola F, et al. Chemotherapy-induced antitumor immunity requires formyl peptide receptor 1. Science. 2015;350(6263):972-8.

13. Sistigu A, Yamazaki T, Vacchelli E, Chaba K, Enot DP, Adam J, et al. Cancer cell-autonomous contribution of type I interferon signaling to the efficacy of chemotherapy. Nat Med. 2014;20(11):1301-9.

14. Gardai SJ, McPhillips KA, Frasch SC, Janssen WJ, Starefeldt A, Murphy-Ullrich JE, et al. Cell-surface calreticulin initiates clearance of viable or apoptotic cells through trans-activation of LRP on the phagocyte. Cell. 2005;123(2):321-34.

15. Zitvogel L, Kepp O, Kroemer G. Decoding cell death signals in inflammation and immunity. Cell. 2010;140(6):798-804.

16. Ma Y, Adjemian S, Mattarollo SR, Yamazaki T, Aymeric L, Yang H, et al. Anticancer chemotherapy-induced intratumoral recruitment and differentiation of antigen-presenting cells. Immunity. 2013;38(4):729-41.

17. Vacchelli E, Sistigu A, Yamazaki T, Vitale I, Zitvogel L, Kroemer G. Autocrine signaling of type 1 interferons in successful anticancer chemotherapy. Oncoimmunology. 2015;4(8):e988042.

18. Walton J, Blagih J, Ennis D, Leung E, Dowson S, Farquharson M, et al. CRISPR/Cas9-Mediated Trp53 and Brca2 Knockout to Generate Improved Murine Models of Ovarian High-Grade Serous Carcinoma. Cancer Res. 2016;76(20):6118-29.

19. Kim J, Coffey DM, Ma L, Matzuk MM. The ovary is an alternative site of origin for high-grade serous ovarian cancer in mice. Endocrinology. 2015;156(6):1975-81.

20. Crowley LC, Marfell BJ, Scott AP, Waterhouse NJ. Quantitation of Apoptosis and Necrosis by Annexin V Binding, Propidium Iodide Uptake, and Flow Cytometry. Cold Spring Harb Protoc. 2016;2016(11).

21. Wei Y, Wang D, Jin F, Bian Z, Li L, Liang H, et al. Pyruvate kinase type M2 promotes tumour cell exosome release via phosphorylating synaptosome-associated protein 23. Nat Commun. 2017;8:14041.

22. Angelova PR, Kasymov V, Christie I, Sheikhbahaei S, Turovsky E, Marina N, et al. Functional Oxygen Sensitivity of Astrocytes. J Neurosci. 2015;35(29):10460-73.

23. Humeau J, Levesque S, Kroemer G, Pol JG. Gold Standard Assessment of Immunogenic Cell Death in Oncological Mouse Models. Methods Mol Biol. 2019;1884:297-315.

24. Ahmed AA, Mills AD, Ibrahim AE, Temple J, Blenkiron C, Vias M, et al. The extracellular matrix protein TGFBI induces microtubule stabilization and sensitizes ovarian cancers to paclitaxel. Cancer Cell. 2007;12(6):514-27.

25. Aran D, Hu Z, Butte AJ. xCell: digitally portraying the tissue cellular heterogeneity landscape. Genome Biol. 2017;18(1):220.

26. Lau TS, Chung TK, Cheung TH, Chan LK, Cheung LW, Yim SF, et al. Cancer cell-derived lymphotoxin mediates reciprocal tumour-stromal interactions in human ovarian cancer by inducing CXCL11 in fibroblasts. J Pathol. 2014;232(1):43-56.

27. Kepp O, Galluzzi L, Martins I, Schlemmer F, Adjemian S, Michaud M, et al. Molecular determinants of immunogenic cell death elicited by anticancer chemotherapy. Cancer Metastasis Rev. 2011;30(1):61-9.

28. Panaretakis T, Kepp O, Brockmeier U, Tesniere A, Bjorklund AC, Chapman DC, et al. Mechanisms of pre-apoptotic calreticulin exposure in immunogenic cell death. EMBO J. 2009;28(5):578-90.

29. Martins I, Kepp O, Schlemmer F, Adjemian S, Tailler M, Shen S, et al. Restoration of the immunogenicity of cisplatin-induced cancer cell death by endoplasmic reticulum stress. Oncogene. 2011;30(10):1147-58.

30. Kepp O, Senovilla L, Vitale I, Vacchelli E, Adjemian S, Agostinis P, et al. Consensus guidelines for the detection of immunogenic cell death. Oncoimmunology. 2014;3(9):e955691.

31. Jordan MA, Toso RJ, Thrower D, Wilson L. Mechanism of mitotic block and inhibition of cell proliferation by taxol at low concentrations. Proc Natl Acad Sci U S A. 1993;90(20):9552-6.

32. Mekhail TM, Markman M. Paclitaxel in cancer therapy. Expert Opin Pharmacother. 2002;3(6):755-66.

33. Weaver BA. How Taxol/paclitaxel kills cancer cells. Mol Biol Cell. 2014;25(18):2677-81.

34. Takeda K, Akira S. TLR signaling pathways. Semin Immunol. 2004;16(1):3-9.

35. Rajput S, Volk-Draper LD, Ran S. TLR4 is a novel determinant of the response to paclitaxel in breast cancer. Mol Cancer Ther. 2013;12(8):1676-87.

36. Szajnik M, Szczepanski MJ, Czystowska M, Elishaev E, Mandapathil M, Nowak-Markwitz E, et al. TLR4 signaling induced by lipopolysaccharide or paclitaxel regulates tumor survival and chemoresistance in ovarian cancer. Oncogene. 2009;28(49):4353-63.

37. Matsunaga N, Tsuchimori N, Matsumoto T, Ii M. TAK-242 (resatorvid), a small-molecule inhibitor of Toll-like receptor (TLR) 4 signaling, binds selectively to TLR4 and interferes with interactions between TLR4 and its adaptor molecules. Mol Pharmacol. 2011;79(1):34-41.

38. Akira S, Takeda K. Toll-like receptor signalling. Nat Rev Immunol. 2004;4(7):499-511.

39. Piras V, Selvarajoo K. Beyond MyD88 and TRIF Pathways in Toll-Like Receptor Signaling. Front Immunol. 2014;5:70.

40. Ma Y, Mattarollo SR, Adjemian S, Yang H, Aymeric L, Hannani D, et al. CCL2/CCR2-dependent recruitment of functional antigen-presenting cells into tumors upon chemotherapy. Cancer Res. 2014;74(2):436-45.

41. Hildebrand DG, Alexander E, Horber S, Lehle S, Obermayer K, Munck NA, et al. IkappaBzeta is a transcriptional key regulator of CCL2/MCP-1. J Immunol. 2013;190(9):4812-20.

42. Willems M, Dubois N, Musumeci L, Bours V, Robe PA. IkappaBzeta: an emerging player in cancer. Oncotarget. 2016;7(40):66310-22.

43. Atkins C, Liu Q, Minthorn E, Zhang SY, Figueroa DJ, Moss K, et al. Characterization of a novel PERK kinase inhibitor with antitumor and antiangiogenic activity. Cancer Res. 2013;73(6):1993-2002.

44. Meares GP, Liu Y, Rajbhandari R, Qin H, Nozell SE, Mobley JA, et al. PERK-dependent activation of JAK1 and STAT3 contributes to endoplasmic reticulum stress-induced inflammation. Mol Cell Biol. 2014;34(20):3911-25.

45. Zitvogel L, Kepp O, Senovilla L, Menger L, Chaput N, Kroemer G. Immunogenic tumor cell death for optimal anticancer therapy: the calreticulin exposure pathway. Clin Cancer Res. 2010;16(12):3100-4.

46. Martins I, Kepp O, Galluzzi L, Senovilla L, Schlemmer F, Adjemian S, et al. Surface-exposed calreticulin in the interaction between dying cells and phagocytes. Ann N Y Acad Sci. 2010;1209:77-82.

47. Nair-Gupta P, Baccarini A, Tung N, Seyffer F, Florey O, Huang Y, et al. TLR signals induce phagosomal MHC-I delivery from the endosomal recycling compartment to allow cross-presentation. Cell. 2014;158(3):506-21.

48. Suzuki K, Verma IM. Phosphorylation of SNAP-23 by IkappaB kinase 2 regulates mast cell degranulation. Cell. 2008;134(3):485-95.

49. Karim ZA, Zhang J, Banerjee M, Chicka MC, Al Hawas R, Hamilton TR, et al. IkappaB kinase phosphorylation of SNAP-23 controls platelet secretion. Blood. 2013;121(22):4567-74.

50. Zasadil LM, Andersen KA, Yeum D, Rocque GB, Wilke LG, Tevaarwerk AJ, et al. Cytotoxicity of paclitaxel in breast cancer is due to chromosome missegregation on multipolar spindles. Sci Transl Med. 2014;6(229):229ra43.

51. Jordan MA, Wilson L. Microtubules as a target for anticancer drugs. Nat Rev Cancer. 2004;4(4):253-65.

52. Peng J, Hamanishi J, Matsumura N, Abiko K, Murat K, Baba T, et al. Chemotherapy Induces Programmed Cell Death-Ligand 1 Overexpression via the Nuclear Factor-kappaB to Foster an Immunosuppressive Tumor Microenvironment in Ovarian Cancer. Cancer Res. 2015;75(23):5034-45.

53. Bezu L, Sauvat A, Humeau J, Gomes-da-Silva LC, Iribarren K, Forveille S, et al. eIF2alpha phosphorylation is pathognomonic for immunogenic cell death. Cell Death Differ. 2018;25(8):1375-93.

54. Senovilla L, Vitale I, Martins I, Tailler M, Pailleret C, Michaud M, et al. An immunosurveillance mechanism controls cancer cell ploidy. Science. 2012;337(6102):1678-84.

55. Wanderley CW, Colon DF, Luiz JPM, Oliveira FF, Viacava PR, Leite CA, et al. Paclitaxel Reduces Tumor Growth by Reprogramming Tumor-Associated Macrophages to an M1 Profile in a TLR4-Dependent Manner. Cancer Res. 2018;78(20):5891-900.

56. Ahrens S, Zelenay S, Sancho D, Hanc P, Kjaer S, Feest C, et al. F-actin is an evolutionarily conserved damage-associated molecular pattern recognized by DNGR-1, a receptor for dead cells. Immunity. 2012;36(4):635-45.

57. Zhang JG, Czabotar PE, Policheni AN, Caminschi I, Wan SS, Kitsoulis S, et al. The dendritic cell receptor Clec9A binds damaged cells via exposed actin filaments. Immunity. 2012;36(4):646-57.

58. Geijtenbeek TB. Actin' as a death signal. Immunity. 2012;36(4):557-9.

59. Sancho D, Joffre OP, Keller AM, Rogers NC, Martinez D, Hernanz-Falcon P, et al. Identification of a dendritic cell receptor that couples sensing of necrosis to immunity. Nature. 2009;458(7240):899-903.

60. Michaud M, Martins I, Sukkurwala AQ, Adjemian S, Ma Y, Pellegatti P, et al. Autophagy-dependent anticancer immune responses induced by chemotherapeutic agents in mice. Science. 2011;334(6062):1573-7.

61. Ovarian Tumor Tissue Analysis C, Goode EL, Block MS, Kalli KR, Vierkant RA, Chen W, et al. Dose-Response Association of CD8+ Tumor-Infiltrating Lymphocytes and Survival Time in High-Grade Serous Ovarian Cancer. JAMA Oncol. 2017;3(12):e173290.

62. Lo CS, Sanii S, Kroeger DR, Milne K, Talhouk A, Chiu DS, et al. Neoadjuvant Chemotherapy of Ovarian Cancer Results in Three Patterns of Tumor-Infiltrating

Lymphocyte Response with Distinct Implications for Immunotherapy. Clin Cancer Res. 2017;23(4):925-34.

63. Bohm S, Montfort A, Pearce OM, Topping J, Chakravarty P, Everitt GL, et al. Neoadjuvant Chemotherapy Modulates the Immune Microenvironment in Metastases of Tubo-Ovarian High-Grade Serous Carcinoma. Clin Cancer Res. 2016;22(12):3025-36.

64. Fucikova J, Becht E, Iribarren K, Goc J, Remark R, Damotte D, et al. Calreticulin Expression in Human Non-Small Cell Lung Cancers Correlates with Increased Accumulation of Antitumor Immune Cells and Favorable Prognosis. Cancer Res. 2016;76(7):1746-56.

Figure Legends

Figure 1

Paclitaxel induces ICD-associated DAMPs and antitumor immunity in syngeneic murine model of ovarian tumor. **A,** Cell viability assay demonstrating the cell proliferation of ID8 murine ovarian cancer cell line treated with chemotherapeutic drugs including paclitaxel (PTX), cisplatin (CDDP), carboplatin (CBDCA), or mitoxantrone (MTX)) in serial dilutions (0.1 μM to 1000 μM) for 48 hours (left panel). Percentage of growth inhibition was determined by comparing the difference between percentage of viable cells with and without treatment. The half maximal inhibitory concentration 50 (IC50) of each drug was determined and applied to the following experiments unless otherwise specified. Cell death was determined by treating the ID8 cells with respective IC50 of PTX (20 μM), CBDCA (200 μM) or MTX (1 μM) for 48 hours (right panel), while CDDP was minimized at a concentration of 300 μM. The cells were stained with annexin V-FITC (AnnV) and propidium iodide (PI) and examined by flow cytometry. AnnV+PI- represents apoptotic cell death; AnnV-PI+ represents non-apoptotic cell death; AnnV+PI+ represents necrotic cell death. **B,** Surface expressions of CALR and ERp57 on ID8 cells after treatments of PTX (20 μM), CDDP (300 μM), CBDCA (200 μM) and MTX (1 μM) respectively for 48 hours were detected by flow cytometry. **C,** Extracellular ATP (left panel) and intracellular ATP (right panel) concentrations in ID8 cells after drug treatments were detected by ENLITEN ATP Assay and ATP Assay kit respectively. **D,** Soluble HMGB1 in conditioned media of ID8 cells after drug treatments was detected by ELISA (left panel) and Western blot (right panel). **E-G,** Surface expressions of ANXA1 (**E**), HSP70 (**F**) and HSP90 (**G**) on ID8 cells after drug treatments were detected by flow cytometry. **H,** mRNA expressions of Ifnb1 and Cxcl10 in ID8 cells after drug treatments were detected by real-time qRT-PCR. Data shown (**A-H**) are expressed as mean ± S.E.M. from three independent replicates (*** $p<0.001$). DMSO was

served as a vehicle control. **I,** Tumor-free survival curve indicating the antitumor response of paclitaxel-induced ICD on syngeneic mouse model *in vivo*. ID8F3 murine ovarian cancer cells were treated with PTX (20 μM) or DMSO overnight and inoculated subcutaneously into one flank of C57BL/6 mice (n=10 per group). The mice were re-challenged with live ID8F3 cancer cells intraperitoneally 7 days later. The intraperitoneal tumor growth was then monitored.

Figure 2

Paclitaxel requires cancer cell-autonomous TLR4 to induce ICD and antitumor response in murine ovarian tumor. **A,** Surface expressions of CALR (left panel) and ERp57 (right panel) on ID8 wild type (WT) cells and isogenic derivatives ID8 Tlr4-/- (Tlr4 KO 3F/8H/10G) clones after PTX (20 mM) treatment for 48 hours were detected by flow cytometry. Different mean fluorescent intensity (Diff.MFI) values was obtained by subtracting CALR or ERp57 staining with respective IgG staining using the software FlowJo. DMSO was served as vehicle controls. **B-E,** Extracellular ATP concentration (**B**), soluble HMGB1 (**C**), surface expression of ANXA1 (**D**), and mRNA expression of Cxcl10 (**E**) in ID8 WT cells and Tlr4 KO clones after PTX treatment for 48 hours. **F-J,** Surface expressions of CALR (left panel) and ERp57 (right panel) (**F**), extracellular ATP concentration (**G**), soluble HMGB1 (**H**), surface expression of ANXA1 (**I**) and mRNA expression of Cxcl10 (**J**) on ID8 cells with TAK-242 pre-treatment (100 nM) for 6 hours prior to PTX treatment. **K,** Antitumor immunity of ID8F3 Tlr4 KO clones after PTX treatment was examined by tumor vaccination in vivo. ID8F3 Tlr4 KO cells treated overnight with PTX (20 mM) or DMSO were inoculated subcutaneously into the flank of C57BL/6 mice (n=5 per group). The mice were re-challenged with live ID8F3 WT cells intraperitoneally 7 days later. The intraperitoneal tumor growth was monitored.

Figure 3

Paclitaxel activates canonical NF-κB signaling pathway via TLR4/MyD88-dependent pathway; and induces Ccl2 transcription via TLR4/MyD88-mediated NF-κB signaling pathway in murine ovarian cancer cells. **A**, Protein expressions of TLR4, MyD88 and TRIF in ID8 cells after PTX treatment (20 μM) for 1-48 hours was examined by Western blot. β-actin was served as a loading control. **B**, Expressions of p105, p50, RelA (p65) and RelB in the cytoplasmic (Cyto) or nuclear (Nuc) proteins of ID8 cells after PTX treatment for 1-48 hours. **C**-**D**, Protein expressions of p65 in the cytoplasmic or nuclear proteins of ID8 WT cells and Tlr4 KO clones after PTX treatment (**C**) and of ID8 cells with TAK-242 pre-treatment prior to PTX treatment (**D**). **E** and **F**, mRNA expression of Ccl2 in ID8 cells after treatments of PTX (20 μM), CDDP (300 μM), CBDCA (200 μM) and MTX (1 μM) respectively for 48 hours (left panel) and after PTX treatment (20 μM) for 1-48 hours (right panel) (**E**); and in ID8 WT cells and Tlr4 KO clones after PTX treatment for 48 hours (**F**). DMSO was served as vehicle controls. **G,** mRNA expression of Tlr4 in ID8 cells with treatment of Tlr4-specific siRNA (siTlr4) (left panel). mRNA expression of Ccl2 in ID8 cells with pre-treatment of Tlr4-specific siRNA (siTlr4) (middle panel) for 6 hours prior to PTX treatment. Ccl2 promoter activity in ID8 cells with pre-treatment of siTlr4 prior to PTX treatment was determined by luciferase reporter assay (right panel). Absence of siRNA (Mock) and scrambled siRNA (siControl) were served as negative controls. **H,** mRNA expression of Ccl2 in ID8 cells with pre-treatment of TAK-242 for 6 hours prior to PTX treatment. **I-L**, mRNA expression of Nfkbiz (IκBζ) in ID8 cells after PTX treatment for 1-48 hours (**I**); in ID8 WT cells and ID8 Tlr4 KO clones after PTX treatment for 48 hours (**J**); and in ID8 cells with pre-treatment of siTlr4 (**K**) and TAK-242 prior to PTX treatment (**L**). **M,** Expression of p65 in the cytoplasmic and nuclear proteins of ID8 cells with pre-treatment of

BAY-11-7082 (100 nM) for 6 hours prior to PTX treatment. **N**, mRNA expressions of Ccl2 (left panel) and Nfkbiz (right panel) in ID8 cells with pre-treatment of BAY-11-7082 prior to PTX treatment. **O**, Ccl2 promoter activity in ID8 cells with pre-treatment of BAY-11-7082 prior to PTX treatment.

Figure 4

Paclitaxel induces PERK activation and eIF2α phosphorylation in murine ovarian cancer cells independent of TLR4. **A-F**, Protein expressions of PERK, eIF2α, and phosphorylated-eIF2α (p-eIF2α) in ID8 cells after treatments of PTX (20 μM), CDDP (300 μM), CBDCA (200 μM) and MTX (1 μM) respectively for 48 hours. DMSO was served as a vehicle control (**A**); in ID8 and TKO cells after PTX treatment (20 μM) for 1-48 hours (**B, C**); in ID8 WT cells and Tlr4 KO clones after PTX treatment for 48 hours (**D**); in ID8 WT cells and Tlr4 KO clones with MTX treatment (1 μM) for 48 hours (**E**); and in ID8 cells with TAK-242 pre-treatment prior to PTX treatment (**F**).

Figure 5

Paclitaxel induces SNARE-dependent exocytosis of ATP-containing vesicles in murine ovarian cancer cells via TLR4-mediated IKK2 activation. **A-C**, Protein expression of IKK2 and phosphorylated-IKK2 (p-IKK2) in ID8 cells after PTX treatment (20 μM) for 1-48 hours **(A)**; in ID8 wild type cells and ID8 Tlr4 KO clones after treatment PTX treatment **(B)**; and in ID8 cells with pre-treatment of TAK-242 prior to PTX treatment **(C)**. **D**, Protein expression of SNAP23 and phosphorylated-SNAP23 (p-SNAP23) in ID8 cells after PTX treatment for 1-48 hours was determined by Western blot using Phos-tag SDS-PAGE and anti-SNAP23 antibody. AP: alkaline phosphatase treatment was served as a negative control. **E** and **F,** Protein expression of SNAP23 and p-SNAP23 in ID8 WT cells and Tlr4 KO clones after

PTX treatment for 48 hours (**E**) and in ID8 cells with pre-treatment of TAK-242 prior to PTX treatment (**F**). **G,** Protein expressions of IKK2 and p-IKK2 in ID8 cells with pre-treatment of TPCA-1 (100 nM) or IKK2 inhibitor V (100 nM) for 6 hours prior to PTX treatment. DMSO was served as a vehicle control. **H**, Protein expressions of SNAP23 and p-SNAP23 in ID8 cells with pre-treatment of TPCA-1 or IKK2 inhibitor IV prior to PTX treatment. **I**, Surface expressions of CALR (left panel), ERp57 (middle panel) and ANXA-1 (right panel) in ID8 cells with pre-treatment of TPCA-1 prior to PTX treatment. **J** and **K,** Detection of ATP-containing vesicles by quinacrine staining (green) in ID8 WT cells and Tlr4 KO clones after PTX treatment (**J**); and in ID8 cells with pre-treatment of TAK-242 or TPCA-1 prior to PTX treatment (**K**). Nuclei were counterstained with DAPI (blue).

Figure 6

Paclitaxel induces ICD-associated DAMPs and antitumor immunity in human ovarian cancer. **A,** Surface expressions of CALR (top left) and ERp57 (top right), extracellular ATP concentration (bottom left), intracellular ATP concentration (bottom middle) and soluble HMGB1 (bottom right) in SKOV3 human ovarian cancer cells after PTX (20 μM) treatment for 48 hours. DMSO was served as vehicle controls. **B**, Immune cell profiling in the ovarian tumor microenvironment of pre- and post-paclitaxel monotherapy samples in GSE15622 dataset was examined by xCell pipeline. In the dataset (with data from a total of 20 ovarian patients), 14 of the patients had biopsies performed before and after 3 cycles of paclitaxel monotherapy. Volcano plots showed the gene expression enrichment scores (ES) of a total of 33 immune cell types in the post- vs. pre-paclitaxel biopsies of the resistant (n=3; left) and responsive (n=11; right) patients. Red circles represent significant upregulated immune cell types after paclitaxel monotherapy; blue circles represent significant downregulated immune cell types after paclitaxel monotherapy; and grey circles represent the immune cell types with

no significant difference after paclitaxel monotherapy. $p<0.05$ (orange line) and fold change <-2 (blue line) or >+2 (red line) were regarded as significant. **C**, Expressions of cytotoxic T cells and dendritic cells (DCs) in post-NACT and primary ovarian tumors were demonstrated by multiple IHC of CD8, IFN-γ and CD208 using Opal IHC reagents and Mantra Quantitative Pathology Workstation. Representative images of multiple IHC of primary ovarian tumors without NACT (top left), post-NACT tumor with carboplatin monotherapy (top middle) and post-NACT tumors with paclitaxel-carboplatin regimen (top right) were shown. CD8+ T cells were labelled in red; CD208+ DCs were labelled in yellow; IFNγ+ cells were labelled as cyan (200x magnification). Cell densities of CD8+ T cells, IFNγ+ cells, IFNγ+CD8+ T cells and CD208+ DCs in primary and post-NACT ovarian tumors were analyzed and compared by inForm image analysis software (bottom). Green squares represent the data of a post-NACT sample from the patient with NACT carboplatin monotherapy. **D**, Correlations between the gene expression enrichment scores of different T cell subtypes (including CD8+ T cells, CD8+ Tem cells, CD4+ Tem cells, CD8+ Tcm cells, and CD4+ naïve T cells) and mRNA expression levels of TLR4 in post-paclitaxel monotherapy samples of responsive patients (n=11) by Spearman's correlation. **E**, Protein expressions of TLR4 (left panel) and CALR (right panel) in the primary tumors of patients with epithelial ovarian cancer (EOC; n=124) by IHC. Positive signals of TLR4 in cytoplasm and CALR on surface membrane of cancer cells were quantified as H scores by inForm software. Representative images of the tumors with low, medium, and high levels of TLR4 cytoplasmic expression (top left) and CALR surface expression (top right) were shown (200x magnification). Overall survival (OS) and disease-free survival (DFS) of patients with high levels of TLR4 (n=43) comparing to those with low/medium levels of TLR4 (n=81) (bottom left) and patients with high levels of CALR (n=42) comparing to those with low/medium levels of CALR (n=82) (bottom right) were analyzed by Kaplan-Meier survival analysis and

log-rank test. **F**, Comparison of mRNA expression levels of CALR (log2 RMA-signal) between the pre-chemotherapy samples of patients who were resistant to paclitaxel monotherapy (n=7 in GSE15622 study) and those who responded to paclitaxel monotherapy (n=13 in GSE15622 study). **G**, Donut charts showing chemotherapy responses (responsive in red; partial responsive in blue; resistant in grey) of patients with $CALR^{low/medium}$ EOC (n=82; top left) and patients with $CALR^{high}$ EOC (n=42; top right). Correlations between chemotherapy responses (responsive, partial responsive, or resistant) and CALR surface expression levels ($CALR^{low/medium}$ or $CALR^{high}$) in the cancer cells of patients with EOC (n=124) were analyzed by Chi-square test (bottom panel).

Figure 7

Paclitaxel induces ICD in ovarian cancer through TLR4-independent and -dependent pathways. A schematic diagram showing 1) paclitaxel induces mitotic arrest, cell death as well as ER stress via TLR4-independent pathways; 2) paclitaxel induces Ccl2 (likewise Cxcl10) upregulation via TLR4/MyD88-NFκB pathways; and 3) paclitaxel induces SNARE-dependent vesicle exocytosis via TLR4-mediated IKK2 activation. The paclitaxel-induced vesicle exocytosis is considered to be essential to the release of ICD-associated DAMPs (including CALR exposure, ATP secretion, HMGB1 release, ANXA1 exposure and CXCL10 expression).

Figures

Figure 1. Paclitaxel induces ICD-associated DAMPs and antitumor immunity in syngeneic murine model of ovarian tumor.

Figure 2. Paclitaxel requires cancer cell-autonomous TLR4 to induce ICD and antitumor response in murine ovarian tumor.

Figure 3. Paclitaxel activates canonical NF-κB signaling pathway via TLR4/MyD88-dependent pathway; and induces Ccl2 transcription via TLR4/MyD88-mediated NF-κB signaling pathway in murine ovarian cancer cells.

Figure 4. Paclitaxel induces PERK activation and eIF2α phosphorylation in murine ovarian cancer cells independent of TLR4.

Figure 5. Paclitaxel induces SNARE-dependent exocytosis of ATP-containing vesicles in murine ovarian cancer cells via TLR4-mediated IKK2 activation.

Figure 6. Paclitaxel induces ICD-associated DAMPs and antitumor immunity in human ovarian cancer.

Figure 1

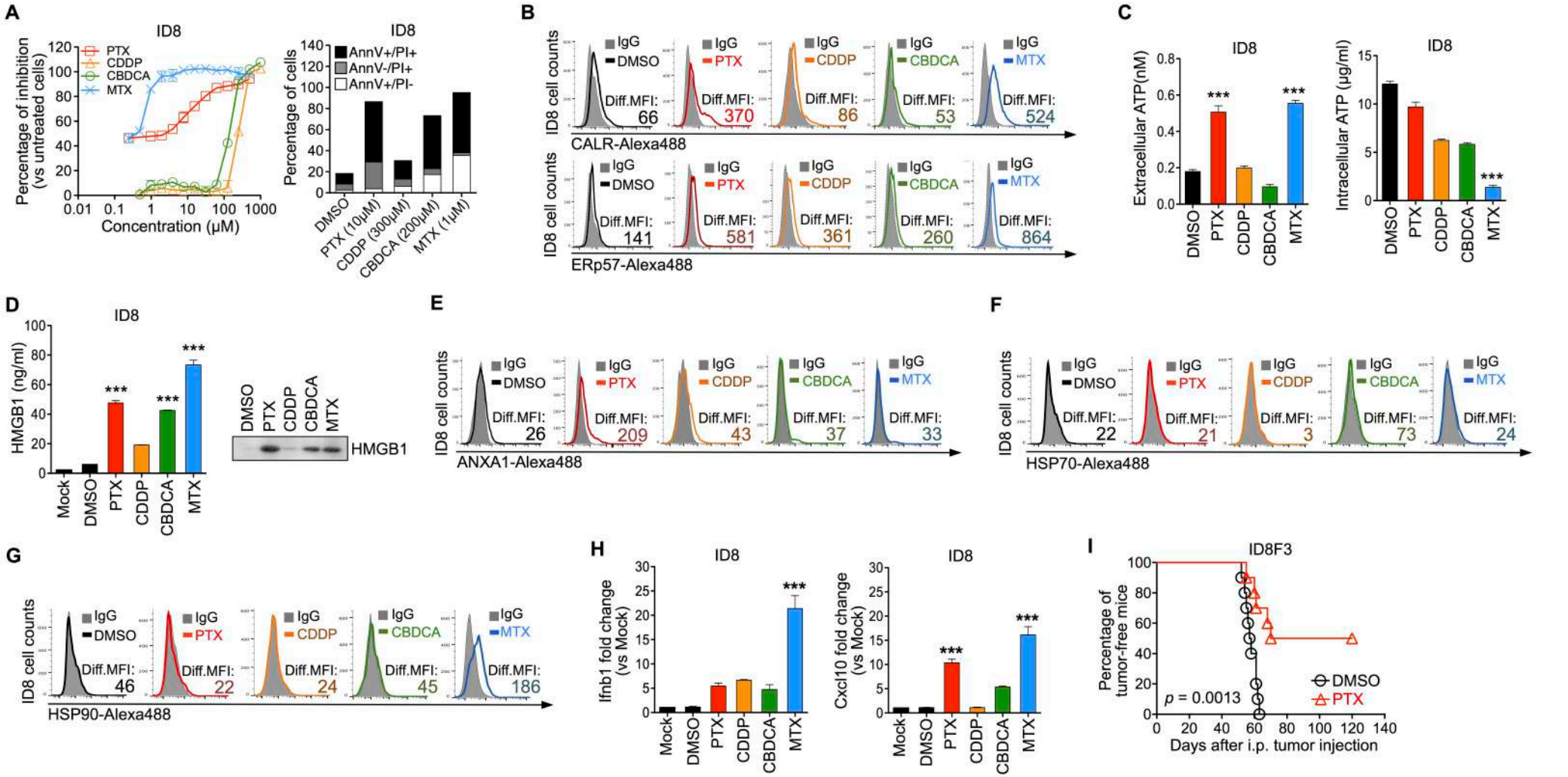
A
ID8
PTX
CDDP
CBDCA
MTX
Percentage of inhibition (vs untreated cells)
Concentration (μM)
ID8
AnnV+/PI+
AnnV-/PI+
AnnV+/PI-
Percentage of cells
DMSO
PTX (10μM)
CDDP (300μM)
CBDCA (200μM)
MTX (1μM)
B
ID8 cell counts
IgG
DMSO
PTX
CDDP
CBDCA
MTX
Diff.MFI:
66
370
86
53
524
CALR-Alexa488
141
581
361
260
864
ERp57-Alexa488
C
ID8
Extracellular ATP(nM)
Intracellular ATP (μg/ml)
***
DMSO
PTX
CDDP
CBDCA
MTX
D
ID8
HMGB1 (ng/ml)
Mock
HMGB1
E
ANXA1-Alexa488
26
209
43
37
33
F
HSP70-Alexa488
22
21
3
73
24
G
HSP90-Alexa488
46
22
24
45
186
H
ID8
Ifnb1 fold change (vs Mock)
Cxcl10 fold change (vs Mock)
I
ID8F3
Percentage of tumor-free mice
p = 0.0013
Days after i.p. tumor injection

Figure 2

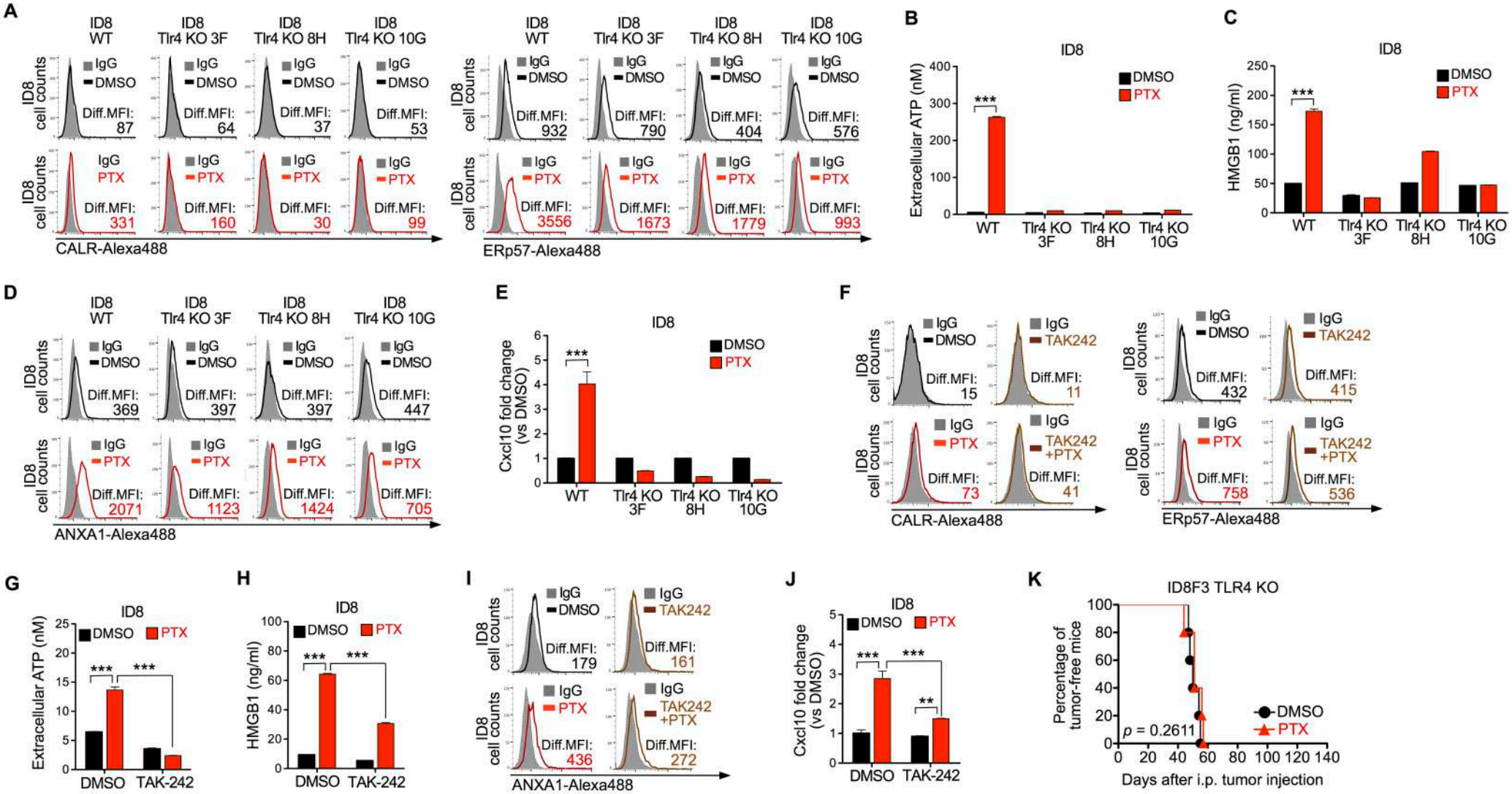
A
ID8 WT
ID8 Tlr4 KO 3F
ID8 Tlr4 KO 8H
ID8 Tlr4 KO 10G
ID8 cell counts
IgG
DMSO
PTX
Diff.MFI:
87
64
37
53
331
160
30
99
932
790
404
576
3556
1673
1779
993
CALR-Alexa488
ERp57-Alexa488
B
ID8
Extracellular ATP (nM)
***
DMSO
PTX
WT
Tlr4 KO 3F
Tlr4 KO 8H
Tlr4 KO 10G
C
ID8
HMGB1 (ng/ml)
***
D
ID8 WT
ID8 Tlr4 KO 3F
ID8 Tlr4 KO 8H
ID8 Tlr4 KO 10G
Diff.MFI:
369
397
397
447
2071
1123
1424
705
ANXA1-Alexa488
E
ID8
Cxcl10 fold change (vs DMSO)
***
F
TAK242
TAK242 +PTX
15
11
73
41
432
415
758
536
CALR-Alexa488
ERp57-Alexa488
G
ID8
Extracellular ATP (nM)
***
***
DMSO
TAK-242
H
ID8
HMGB1 (ng/ml)
I
TAK242
TAK242 +PTX
179
161
436
272
ANXA1-Alexa488
J
ID8
Cxcl10 fold change (vs DMSO)
***
***
**
K
ID8F3 TLR4 KO
Percentage of tumor-free mice
p = 0.2611
DMSO
PTX
Days after i.p. tumor injection

Figure 3

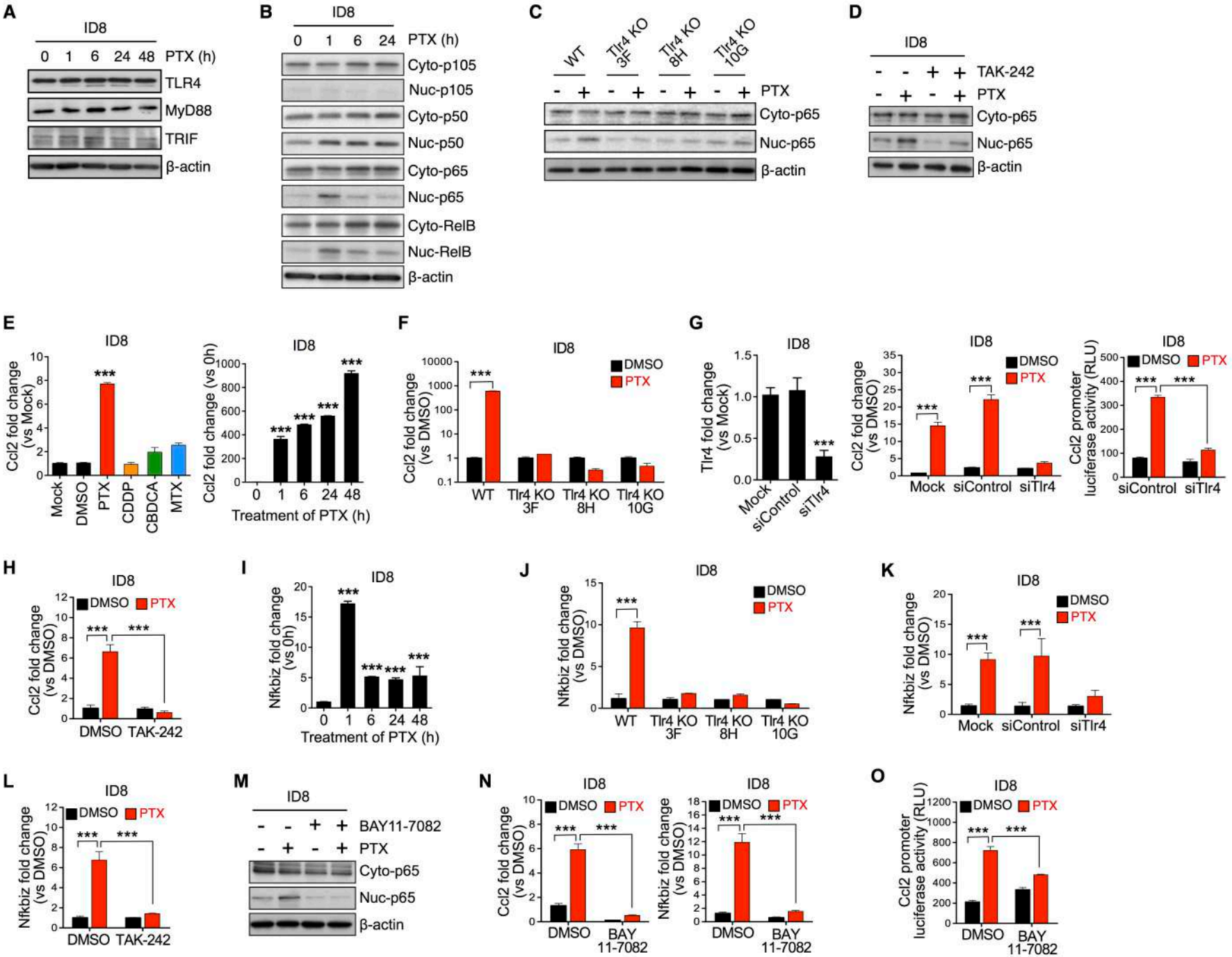
A
ID8
0 1 6 24 48 PTX (h)
TLR4
MyD88
TRIF
β-actin
B
ID8
0 1 6 24 PTX (h)
Cyto-p105
Nuc-p105
Cyto-p50
Nuc-p50
Cyto-p65
Nuc-p65
Cyto-RelB
Nuc-RelB
β-actin
C
WT
Tlr4 KO 3F
Tlr4 KO 8H
Tlr4 KO 10G
PTX
Cyto-p65
Nuc-p65
β-actin
D
ID8
TAK-242
PTX
Cyto-p65
Nuc-p65
β-actin
E
ID8
Ccl2 fold change (vs Mock)
Mock DMSO PTX CDDP CBDCA MTX
Ccl2 fold change (vs 0h)
Treatment of PTX (h)
F
ID8
DMSO PTX
Ccl2 fold change (vs DMSO)
WT Tlr4 KO 3F Tlr4 KO 8H Tlr4 KO 10G
G
ID8
Tlr4 fold change (vs Mock)
Mock siControl siTlr4
Ccl2 fold change (vs DMSO)
Ccl2 promoter luciferase activity (RLU)
H
ID8
Ccl2 fold change (vs DMSO)
DMSO TAK-242
I
ID8
Nfkbiz fold change (vs 0h)
Treatment of PTX (h)
J
ID8
Nfkbiz fold change (vs DMSO)
K
ID8
Nfkbiz fold change (vs DMSO)
L
ID8
Nfkbiz fold change (vs DMSO)
M
ID8
BAY11-7082
PTX
Cyto-p65
Nuc-p65
β-actin
N
ID8
Ccl2 fold change (vs DMSO)
Nfkbiz fold change (vs DMSO)
DMSO BAY 11-7082
O
ID8
Ccl2 promoter luciferase activity (RLU)
DMSO BAY 11-7082

Figure 4

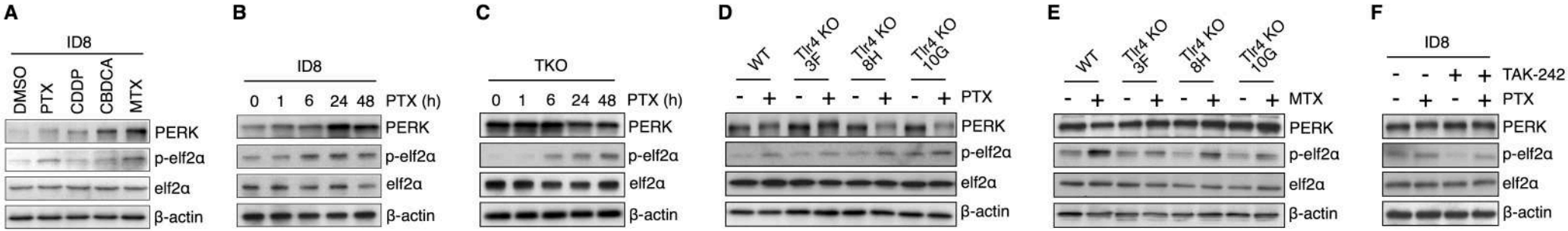
A
ID8
DMSO
PTX
CDDP
CBDCA
MTX
PERK
p-elf2α
elf2α
β-actin
B
ID8
0 1 6 24 48 PTX (h)
PERK
p-elf2α
elf2α
β-actin
C
TKO
0 1 6 24 48 PTX (h)
PERK
p-elf2α
elf2α
β-actin
D
WT
Tlr4 KO 3F
Tlr4 KO 8H
Tlr4 KO 10G
- + - + - + - + PTX
PERK
p-elf2α
elf2α
β-actin
E
WT
Tlr4 KO 3F
Tlr4 KO 8H
Tlr4 KO 10G
- + - + - + - + MTX
PERK
p-elf2α
elf2α
β-actin
F
ID8
- - + + TAK-242
- + - + PTX
PERK
p-elf2α
elf2α
β-actin

Figure 5

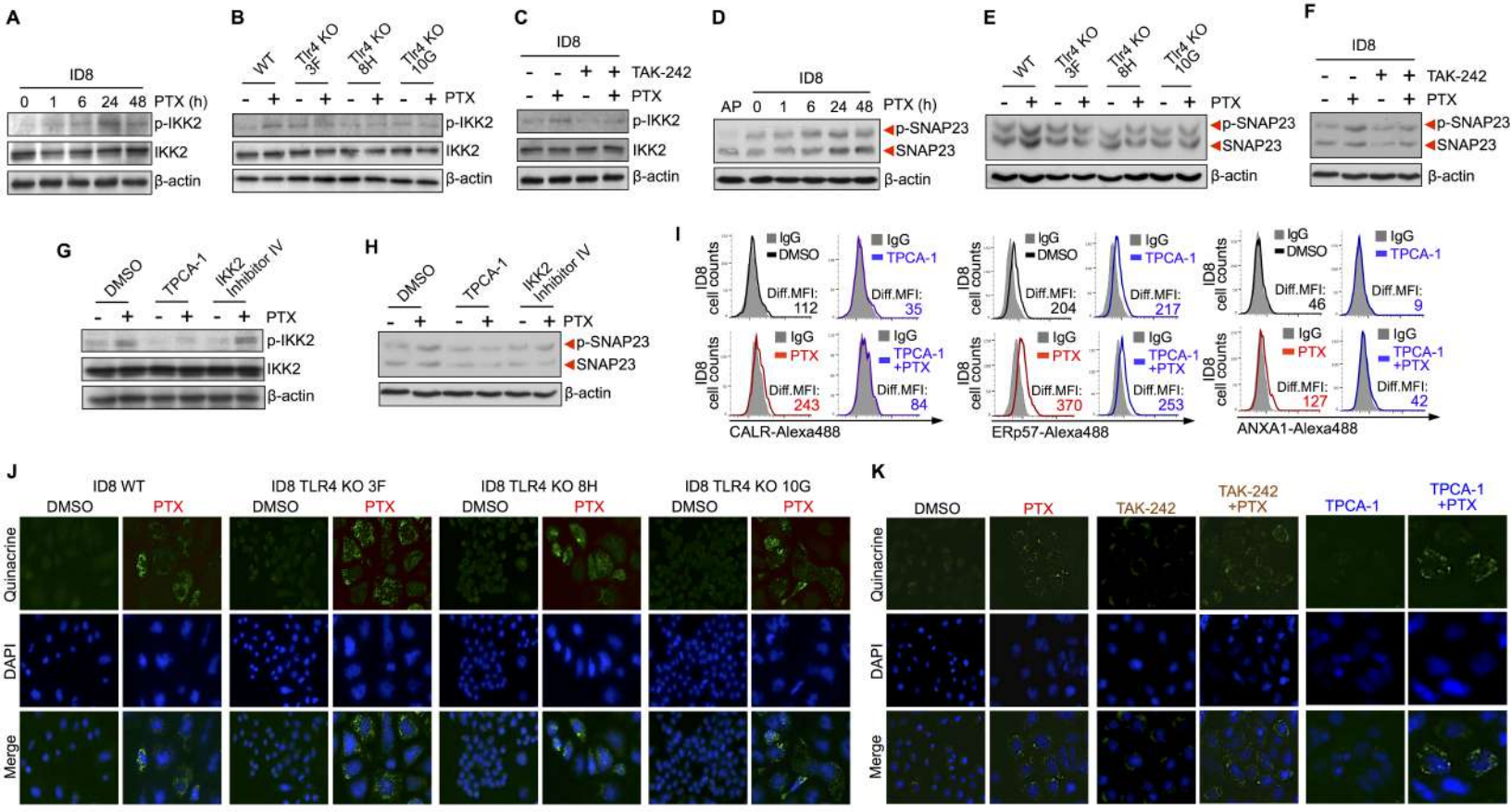
A
ID8
0 1 6 24 48 PTX (h)
p-IKK2
IKK2
β-actin
B
WT
Tlr4 KO 3F
Tlr4 KO 8H
Tlr4 KO 10G
PTX
p-IKK2
IKK2
β-actin
C
ID8
TAK-242
PTX
p-IKK2
IKK2
β-actin
D
ID8
AP 0 1 6 24 48 PTX (h)
p-SNAP23
SNAP23
β-actin
E
WT
Tlr4 KO 3F
Tlr4 KO 8H
Tlr4 KO 10G
PTX
p-SNAP23
SNAP23
β-actin
F
ID8
TAK-242
PTX
p-SNAP23
SNAP23
β-actin
G
DMSO
TPCA-1
IKK2 Inhibitor IV
PTX
p-IKK2
IKK2
β-actin
H
DMSO
TPCA-1
IKK2 Inhibitor IV
PTX
p-SNAP23
SNAP23
β-actin
I
ID8 cell counts
IgG
DMSO
TPCA-1
PTX
TPCA-1 +PTX
Diff.MFI: 112
Diff.MFI: 35
Diff.MFI: 243
Diff.MFI: 84
CALR-Alexa488
Diff.MFI: 204
Diff.MFI: 217
Diff.MFI: 370
Diff.MFI: 253
ERp57-Alexa488
Diff.MFI: 46
Diff.MFI: 9
Diff.MFI: 127
Diff.MFI: 42
ANXA1-Alexa488
J
ID8 WT
ID8 TLR4 KO 3F
ID8 TLR4 KO 8H
ID8 TLR4 KO 10G
DMSO
PTX
Quinacrine
DAPI
Merge
K
DMSO
PTX
TAK-242
TAK-242 +PTX
TPCA-1
TPCA-1 +PTX
Quinacrine
DAPI
Merge

Figure 6

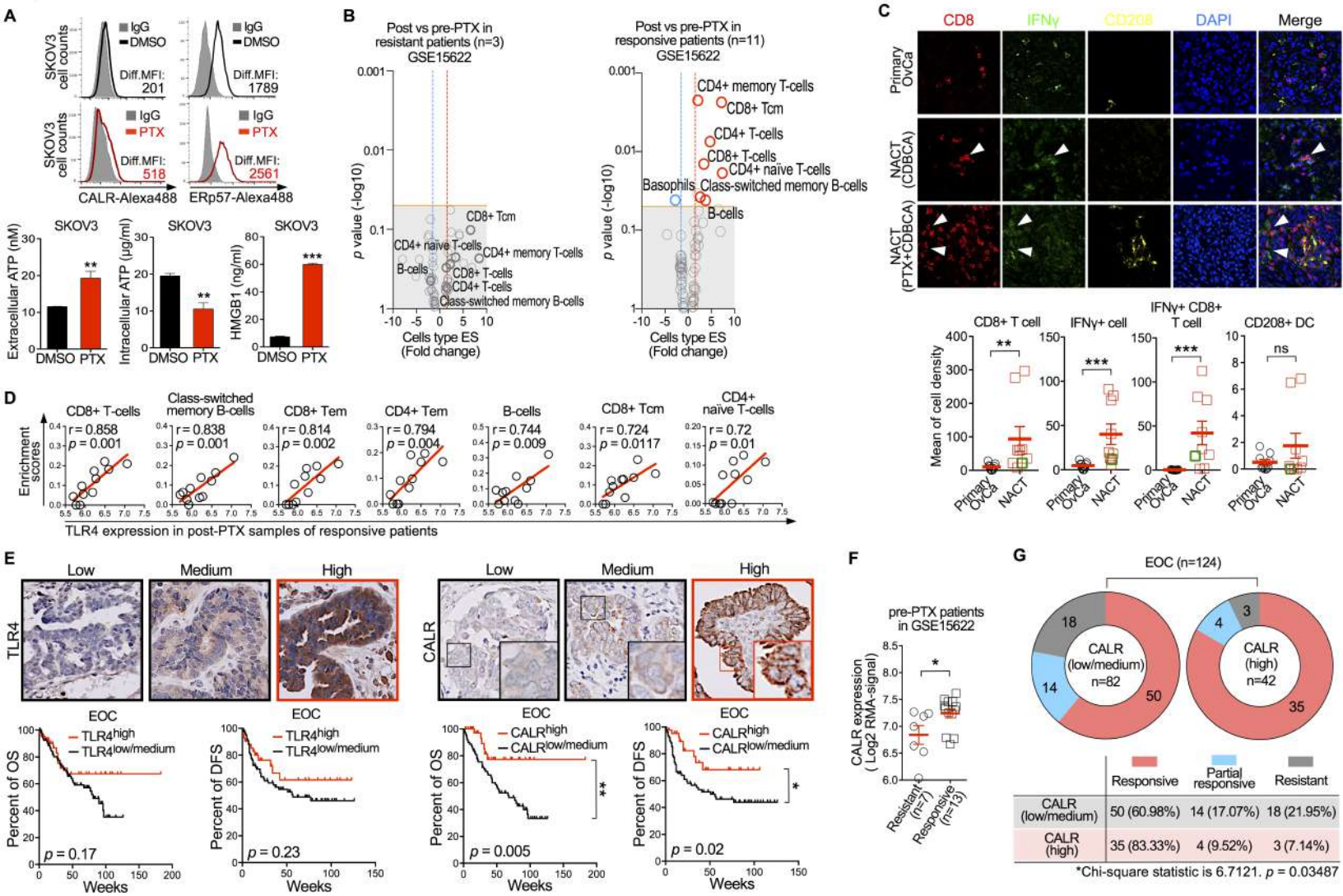
A
SKOV3 cell counts
IgG
DMSO
Diff.MFI: 201
Diff.MFI: 1789
PTX
Diff.MFI: 518
Diff.MFI: 2561
CALR-Alexa488
ERp57-Alexa488
SKOV3
Extracellular ATP (nM)
Intracellular ATP (µg/ml)
HMGB1 (ng/ml)
DMSO PTX
B
Post vs pre-PTX in resistant patients (n=3) GSE15622
Post vs pre-PTX in responsive patients (n=11) GSE15622
p value (-log10)
Cells type ES (Fold change)
CD8+ Tcm
CD4+ naive T-cells
CD4+ memory T-cells
B-cells
CD8+ T-cells
CD4+ T-cells
Class-switched memory B-cells
Basophils
CD4+ naïve T-cells
C
CD8
IFNγ
CD208
DAPI
Merge
Primary OvCa
NACT (CDBCA)
NACT (PTX+CDBCA)
Mean of cell density
CD8+ T cell
IFNγ+ cell
IFNγ+ CD8+ T cell
CD208+ DC
ns
D
Enrichment scores
CD8+ T-cells
Class-switched memory B-cells
CD8+ Tem
CD4+ Tem
B-cells
CD8+ Tcm
CD4+ naïve T-cells
r = 0.858 p = 0.001
r = 0.838 p = 0.001
r = 0.814 p = 0.002
r = 0.794 p = 0.004
r = 0.744 p = 0.009
r = 0.724 p = 0.0117
r = 0.72 p = 0.01
TLR4 expression in post-PTX samples of responsive patients
E
Low
Medium
High
TLR4
CALR
EOC
TLR4high
TLR4low/medium
CALRhigh
CALRlow/medium
Percent of OS
Percent of DFS
p = 0.17
p = 0.23
p = 0.005
p = 0.02
Weeks
F
pre-PTX patients in GSE15622
CALR expression (Log2 RMA-signal)
Resistant (n=7)
Responsive (n=13)
G
EOC (n=124)
CALR (low/medium) n=82
CALR (high) n=42
18
14
50
4
3
35
Responsive
Partial responsive
Resistant
CALR (low/medium) 50 (60.98%) 14 (17.07%) 18 (21.95%)
CALR (high) 35 (83.33%) 4 (9.52%) 3 (7.14%)
*Chi-square statistic is 6.7121. p = 0.03487

Figure 7

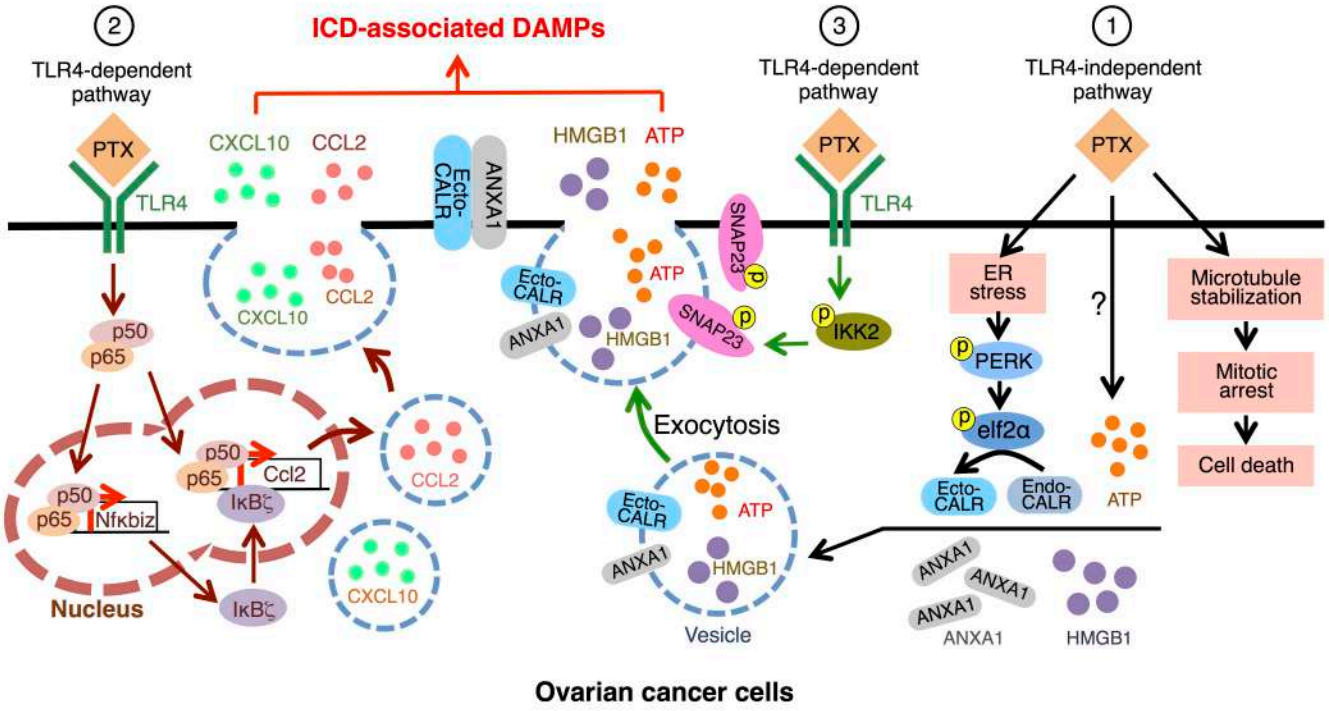
2
TLR4-dependent pathway
PTX
TLR4
ICD-associated DAMPs
CXCL10
CCL2
Ecto-CALR
ANXA1
HMGB1
ATP
3
TLR4-dependent pathway
PTX
TLR4
1
TLR4-independent pathway
PTX
p50
p65
Nucleus
Nfκbiz
Ccl2
IκBζ
CCL2
CXCL10
SNAP23
P
IKK2
Exocytosis
Vesicle
ER stress
PERK
elf2α
?
Endo-CALR
Microtubule stabilization
Mitotic arrest
Cell death
Ovarian cancer cells